7-1-2015

Drought in the Colorado River Basin: Spatiotemporal Analysis using an Edge Detection Filter

Lindsay Ross

Lindsay A. Ross

Candidate

Earth and Planetary Sciences

Department

This thesis is approved, and it is acceptable in quality and form for publication:

Approved by the Thesis Committee:

Louis A. Scuderi, Chairperson

Peter J. Fawcett

David S. Gutzler

DROUGHT IN THE COLORADO RIVER BASIN: SPATIOTEMPORAL ANALYSIS USING AN EDGE DETECTION FILTER

BY

LINDSAY A. ROSS

B.S., METEOROLOGY, UNIVERSITY OF OKLAHOMA, 2013

THESIS

Submitted in Partial Fulfillment of the
Requirements for the Degree of

Master of Science

Earth and Planetary Sciences

The University of New Mexico
Albuquerque, New Mexico

July 2015

DROUGHT IN THE COLORADO RIVER BASIN: SPATIOTEMPORAL ANALYSIS USING AN EDGE DETECTION FILTER

by

Lindsay A. Ross

B.S., Meteorology, University of Oklahoma, 2013
M.S., Earth and Planetary Science, University of New Mexico, 2015

ABSTRACT

A detailed history of drought variability in the Colorado River Basin for the last half millennium was obtained using tree ring-widths of precipitation sensitive trees as a proxy record of past climatic conditions. A one-dimensional edge detection filter was applied to standardized ring-width indices to identify years with rapid change in ring-width magnitude that may reflect changes in state. Both standardized indices and edge detection outputs were mapped to analyze how the spatial pattern of drought changes over time. A Principal Components Analysis was performed for both the mapped index and edge detection outputs to determine whether there were specific patterns within the data. This data analysis identified repeating spatial patterns between each of the identified drought periods during drought onset, with the first principal component of the edge detection accounting for 60% of the variance in the edge data. A temporal mapping of principal component loadings suggests that the Pacific Decadal Oscillation and the Atlantic Multidecadal Oscillation play a significant role in forcing drought onset patterns. Superposed Epoch Analysis and a species-sensitivity analysis revealed that there are differences that exist between the droughts, including variation in the timing of the peak index year relative to the onset of drought (peak edge year), in magnitude of drought response, and in the migration patterns of drought onset, making it difficult to classify the droughts.

The edge detection filter was found to be successful in identifying periods of drought onset, illustrating drought onset, and capturing migration of drought areas. The Principal Component Analysis loading patterns suggest that there are specific regions within the Colorado River Basin that vary synchronously during drought onset. Having a better understanding of these repeating regional variations in the Colorado River Basin will lead to improved drought predictability, and aid in water management in the region.

TABLE OF CONTENTS

LIST OF FIGURES

LIST OF TABLES

Chapter 1

Introduction

Drought is a recurring natural phenomenon that directly impacts the environment and indirectly impacts the economy. Successive drought years in a region often lead to significant crop failure, and severely reduce water resources both within the drought region and in areas connected hydrologically to the region. In economic terms, drought is one of the costliest natural disasters (Cook et al., 2007). Between 1980 and 2003, drought accounted for 17% of weather related disasters in the United States (U.S.), and was responsible for over 40% of the total cost (Cook et al., 2007). The Western U.S., because of its geographic and climatologic characteristics, is particularly prone to drought (Hidalgo, 2004). In the past, the West has experienced widespread and prolonged droughts, leading to devastating societal and ecological impacts (Cook et al., 2007; Hidalgo, 2004; Woodhouse et al., 2009). General Circulation Models (GCMs) project a reduction in precipitation for areas in the Western U.S. during the 21st century due to a warmer climate influenced by an increase in greenhouse gases (Cayan et al., 2010; IPCC, 2013; Held and Soden, 2006). Water is already a precious resource in this region due to natural aridity and a growing population pressure, and reduced precipitation will likely exacerbate the effects of drought. If GCM projections materialize, Western U.S. society may face deeper and historically more unusual water shortages, and sustainability of current water supplies from the over appropriated Colorado River and similar water resources will become unrealistic (Cayan et al., 2010, Lane et al., 1999; Meko and Woodhouse, 2005).

Understanding the spatial distribution of drought sources (i.e. how drought edges migrate), and quantifying the time scale and onset characteristics both temporally and spatially, are paramount to improving drought predictability and could possibly be used for recognition of specific types of drought. In this study drought is characterized within the Colorado River Basin region since 1500AD, including the initiation and migration of these events using an edge detection filter. A Principal Components Analysis is used to determine the spatial characteristics and variability of drought onset. The study site, hereafter referred to as the Colorado River Basin (CRB), includes the Upper and Lower Colorado River Basins, and portions of the surrounding basins (the Missouri Basin, the Arkansas-White-Red Basin, the Rio Grande Basin, and the Great Basin).

Chapter 2

Scientific Background

Drought & Causal Mechanisms

Drought is a naturally occurring phenomenon that has affected the Western U.S. for millennia (Grissino-Mayer, 1996; Meko et al., 2005; Woodhouse and Overpeck, 1998). Drought is well preserved in tree ring records from precipitation-sensitive trees that are located along the drier limits of the species (Cook et al., 2007; Fritts, 1976; Meko et al., 2007). Some of the precipitation sensitive tree species in the CRB include Ponderosa pine, Douglas fir, and Pinyon pine (Scuderi, 2015; Williams et al., 2010). During the Medieval Climate Anomaly (roughly 900AD-1300AD), tree-ring data suggest that droughts in the CRB were widespread and lasted for decades, only being separated by one or two relatively wet years (Cook et al., 2007; Meko et al., 2007). Droughts within the last century have occurred on average every 25 years, and have typically lasted 5 to 10 years (Cook et al., 2007). The megadroughts that occurred in the mid- to late-12th century and during the late 16th century (Cook et al., 2007; Meko et al., 2007; Stahle et al., 2000; Woodhouse et al., 2009) would have far more devastating impacts on Western U.S. society today. Analysis of drought in the CRB during recent centuries, and the potential for classifying these droughts, will lend itself to possibly classifying the megadroughts of the past, in terms of causal mechanisms, and the potential for such an event occurring in the future. An essential part of understanding this difference in drought variability is having knowledge of the climate of the CRB region, and the mechanisms within the climate system that control it.

The southern CRB (Arizona and New Mexico) receives moisture from the Gulf of California and the Gulf of Mexico due to monsoonal flow (Adams and Comrie, 1997; Sheppard et al., 2002). The region also receives moisture from the Pacific Ocean due to the overlying Westerlies. Monsoonal flow causes a precipitation maximum during the summer months, with precipitation totals in the CRB increasing with elevation due to orographic processes (Adams and Comrie, 1997; Sheppard et al., 2002). A second precipitation maximum occurs in the lower CRB during the winter, when Pacific-track storms carried by the polar jet stream produce a significant snowpack (Sheppard et al., 2002). Spring snowmelt from the winter snowpack is a major source of water for reservoirs in the region, whereas much of the summer monsoonal precipitation evaporates before it can contribute to the groundwater supply (Sheppard et al., 2002). The primary source of moisture for the northern CRB (Colorado, Utah, Wyoming, and Nevada) is the Pacific Ocean. The trajectory of Pacific-track storms arriving in the upper and lower CRB is dependent on sea surface temperature (SST) patterns in the Pacific and Atlantic Oceans (McCabe-Glynn et al., 2013). These SST patterns influence the positions of high- and low-pressure centers in the Northern Pacific Ocean and over the continental U.S. (McCabe-Glynn et al., 2013).

Studies of paleoclimatic proxies and climate model simulations have shown that anomalous states of sea surface temperatures (SSTs) in specific oceanic regions influences drought conditions globally, including the CRB region (Cole and Cook, 1998; Cook et al., 2007; Enfield et al., 2001; Gray et al., 2003; Hoerling and Kumar, 2003; McCabe-Glynn et al., 2013; Tootle et al., 2005). The migration of high- and low-pressure centers due to changing sea surface temperatures (SSTs) is a part of this oceanic oscillation phenomenon.

The El Nino – Southern Oscillation (ENSO) occurs on the shortest timescale with episodic intervals occurring every 2 to 8 years (Cole and Cook, 1998; Tootle et al., 2005). During an El Nino event, SSTs in the eastern and tropical Pacific Ocean are anomalously warm. The increase in SST changes the surface pressure distribution in the tropical Pacific (CPC, 2012). The change in surface pressure along the equator produces a perturbation in the atmospheric circulation features, which can enhance the subtropical jet stream resulting in anomalous precipitation patterns over the continental U.S. (CPC, 2012). The opposite conditions occur during a La Nina event. The trade winds along the equator are enhanced, which results in anomalously cool SSTs appearing along the equator and off the western coast of South America. The oscillation in surface pressure causes a perturbation in atmospheric circulation, which leads to meridional shifts and variations in the sub-tropical and polar jet streams. It should be noted that cooler SSTs during La Nina events are known to be drought-inducing for regions of the western U.S. (Cook et al., 2007; Hoerling and Kumar, 2003).

Other oceanic oscillations that contribute to drought in the continental U.S. are the Pacific Decadal Oscillation (PDO) and the Atlantic Multidecadal Oscillation (AMO) (Enfield et al., 2001; Gray et al., 2003). The PDO occurs in the Northern Pacific Ocean (north of 20°N), and has a SST episodic oscillation of about 15 to 25 years. It is forced by variations in the location and strength of the Aleutian Low (Gray et al., 2003). The negative phase, or cool phase, of PDO is linked to drought in the central and southern

Rocky Mountains (Gray et al., 2003; McCabe-Glynn et al., 2013; Mantua et al., 1997; Tootle et al., 2005).

The AMO occurs in the Northern Atlantic Ocean, and has an episodic oscillation of about 65 to 85 years. The cycle is thought to be associated with fluctuations in the strength of the thermohaline circulation (Gray et al., 2003; Tootle et al., 2005). The warm phase of AMO results in portions of the western U.S. (the central and southern Rocky Mountains) receiving less than normal rainfall (Gray et al., 2003; McCabe-Glynn et al., 2013; Tootle et al., 2005). Tootle et al. (2005) find that both PDO and AMO can work to either enhance or diminish the effects of ENSO. Based on this, it is evident that the occurrence of prolonged, continental-scale droughts, involve complex interactions between the Atlantic and Pacific Oceans (Enfield et al., 2001; Gray, 2003).

Teleconnections between the coupled ocean-atmosphere oscillations and occurrences of global hydrologic anomalies result in known patterns of drought. McCabe et al. (2004) completed analyses of patterns of drought frequency in the U.S. as a result of the states of PDO and AMO, and found that drought frequency in the CRB has the greatest increase during the combination of negative PDO and positive AMO. Fye et al. (2003) reconstructed past pluvial and drought patterns over the U.S. (using tree-ring chronologies) as they relate to the spatial extent and magnitude of the 1930’s and 1950’s droughts, and found that reconstructed drought patterns exhibit similarities in terms of extent and intensity to both the 1930’s and 1950’s droughts. What this study addresses, that others have not, is the spatial pattern associated with drought onset in the CRB.

Analyzing Tree Ring-width as a Proxy

In order to better understand the characteristics of drought, it is necessary to look beyond the period of instrumental record. A method of extending the drought record back into the past is analyzing tree ring-width as a proxy for climate. Tree ring-width properties that make them useful as a proxy for drought are moisture-stress sensitivity, broad spatial coverage, annual resolution (to capture single year droughts), exactly dated (for regional comparison), and chronology lengths of centuries to millennia (Cook et al., 2007; Fritts, 1976).

Ring-width data is collected by sampling at least two core radii per tree to reduce intra-tree variability, and at least 20 trees per site in order to minimize “noise”, introduced by tree-specific environmental factors that are not being studied (Fritts, 1976; Grissino-Mayer, 2014). Site selection depends on what limiting factor, precipitation or temperature, the dendroclimatologist wants to study. Precipitation sensitive sites are typically located at the lower elevational or drier limits of the particular species, whereas temperature sensitive sites are found near or at the upper elevational or latitudinal limits of the species (Fritts, 1976). The core samples are then mounted and sanded to allow for cross-dating and raw ring-width measurement. Cross-dating (matching patterns in the raw ring-widths) allows for the record to be extended back in time, which results in the identification of the exact year that each annual ring was formed (Fritts, 1976; Grissino-Mayer, 2014). The raw ring-widths are measured to the nearest 0.01 millimeter and recorded in digital data files (ITRDB, 2015).

Long-term variations can occur in ring-width growth at frequencies from several decades to several centuries, and these may arise as a result of changes in the tree itself or with respect to changes in environmental conditions. As a tree ages, the annual ring-widths naturally become smaller (Fritts, 1976). This growth trend is most often modeled as a negative exponential function (Fritts, 1976). The process of fitting a negative exponential curve to the raw ring-width data, then dividing each raw ring-width by the corresponding value of the fitted curve for a particular year is called standardization. This allows the large variability in ring-width of the younger, fast-growing tree to be comparable to the reduced variability in ring-with of the older, slow-growing tree (Fritts, 1976). Standardization results in a time series of unit-less tree-ring index values, or growth departures, where the expected index value for any given year is 1. Because ring-width is dependent on the limiting factors of the surrounding environment, such as temperature and precipitation, any change of state in the regional climatic conditions, such as those that take place during a drought, will be evident in the growth rings of trees at a site, regardless of their age (Fritts, 1976).

Parameters other than annual ring-width that have been analyzed with respect to changes in climate are earlywood width, latewood width, and changes in wood density (Fritts, 1976). Earlywood is the portion of the annual ring that is formed during the spring, when the growing season begins. Earlywood is comprised of relatively large cells with thin walls, and appears light in color (Fritts, 1976). Towards the end of summer, growth begins to slow, and latewood is formed. The cells within the latewood are relatively small, and have thick walls, making it appear dark in color (Fritts, 1976). Measuring the width of the earlywood or latewood would relate to the climatic conditions during the spring or summer growing season, respectively (Fritts, 1976). For sites where variations in the environmental conditions of the growing season are more highly correlated to changes in cell structure, measuring maximum wood density would give the most information with regards to the varying climatic conditions (Fritts, 1976). X-ray negatives of the core sample are used to measure the wood density within each annual ring, with the maximum wood density appearing at the end of the growing season (Fritts, 1976).

Drought is difficult to define due to variability in climatic conditions, socioeconomic dynamics, and water demands specific to different locations around the world (Mishra and Singh, 2010). Organizations globally define drought differently according to their specific water needs. For example, the World Meteorological Organization (WMO) defines drought as “a sustained, extended deficiency in precipitation” (WMO, 1986), whereas, The Food and Agriculture Organization (FAO, 1983) of the United Nations defines drought as “the percentage of years when crops fail from the lack of moisture.” In a study of hydrologic drought in the Sacramento and Upper Colorado River basins by Meko and Woodhouse (2005), a joint-drought year (drought in both basins) was defined as a year when both basins were below some defined streamflow threshold. Both Cook et al. (2007) and Fye et al. (2003) define drought based on reconstructed PDSI. In this study, drought is defined based on standardization of the ring-widths, with an index value of 1.0 representing the expected growth of an annual ring throughout the chronology established from the growth function. An occurrence of index values less than 1.0 are considered to indicate drought conditions at a given site.

Edge Detection

The edge detection process focuses on object boundaries, where values are changing rapidly over a short distance (Canny, 1986). In this case, a rapid change in ring-width magnitude over a relatively short time period could be considered an ‘edge’. Lim (1990) describes an edge “as a boundary or contour at which a significant change occurs in some physical aspect of the image,” making the method equivalent to thresholding. In this study, thresholding is equivalent to detecting the boundary that indicates a change in climatic state, either from wet to dry or dry to wet conditions. The extraction of edge features in an image can also be useful for image matching (Ali and Clausi, 2001).

The objective of edge detection is to simplify the analysis of images by reducing the amount of data to be processed and still preserving structural information about existing boundaries (Canny, 1986). In this study, this is accomplished by implementing a one-dimensional edge detection filter with a step impulse response as described by Canny (1986) (Fig. 1).

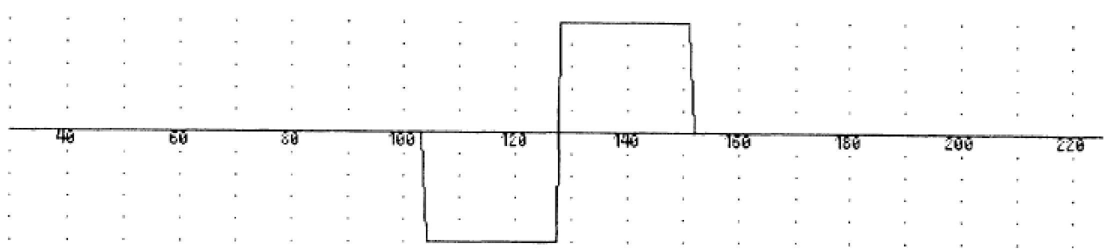

Figure 1. Impulse response of a one-dimensional difference of boxes edge detection filter (Canny, 1986).

It is assumed that the data consists of possible edges plus white Gaussian noise, and for this reason a Gaussian smoothing filter is initially applied to the data (Canny, 1986). For an edge detection filter to be useful, it must meet the following criteria: 1) Good detection, there should be a low probability that the edge filter marks false edges (this criterion corresponds to maximizing signal-to-noise ratio), 2) Good localization – the points marked as edges should be as close as possible to the actual edge, and 3) High sensitivity – only one response to a single edge (Canny, 1986). Canny (1986) states that an edge detection filter with a broad impulse response will have a better signal-to-noise ratio output, whereas a narrow filter will give better localization of edges. This tradeoff between detection and localization performance usually exists when using a step impulse response edge detection filter, however, in this study the Gaussian smoothing filter maximizes the signal-to-noise ratio initially which allows for the use of a narrow, 3-year moving step impulse response edge detection filter.

PDSI

One method of monitoring the spatial and temporal variability of drought is a drought index constructed from climatological data. The Palmer Drought Severity Index (PDSI) is one such index. Developed initially by Palmer in 1965 (Palmer, 1965) in order to assess the severity of drought conditions, it can also be used to document both abnormally dry and abnormally wet conditions (Alley, 1985) and to analyze the characteristics of past droughts. In real time, PDSI is used to monitor drought conditions in order to trigger mitigation strategies if drought conditions become severe.

PDSI was developed using a water balance model approach based on monthly precipitation and temperature data. Other variables included in the water balance model calculation include evapotranspiration, potential evapotranspiration, soil water recharge, potential soil water recharge, runoff, potential runoff, water loss from the soil, and potential water loss from the soil (Alley, 1985; Palmer, 1965). A ratio of the monthly average actual to the monthly average potential is calculated for the set of variables for each month of the year. Given these coefficients, departures between actual precipitation and the Climatically Appropriate for Existing Conditions (CAFEC) precipitation can be calculated for each month and converted into a moisture anomaly index, known as the Palmer Z-Index, which is shown in Equation 1 (Alley, 1985).

$$Z(j) = K_j * d \qquad (1)$$

K_j is a weighting factor for month 'j' that is used to adjust the departure in precipitation (d) so that it is comparable for different areas and different months (Alley, 1985). The Z-Index represents the departure of weather for a particular month from the average climatic conditions for that month (Heim, 2002). PDSI is "an integrator of weather conditions over an extended period of time" because when calculating the PDSI for a particular month the Z-Index for that month and the previous month are taken into account (Alley, 1985). This is shown by Equation 2 (Alley, 1985).

$$PDSI(i) = ((0.897) * PDSI(i-1)) + (Z(i)/3) \qquad (2)$$

Because PDSI is primarily influenced by departures in precipitation it is best at defining when a meteorological drought has occurred (Heim, 2002), defined as "a sustained, extended deficiency in precipitation" by the WMO (1986). The onset and termination of such an event is calculated based on the probability that the dry (or wet) spell has started or ended (Heim, 2002). A lag exists from the time a meteorological drought ends and the time that it takes for the environment to recover from drought conditions; therefore, the PDSI can indicate that a drought event has ended even if hydrological drought, defined as a period of inadequate water resources for the established water uses in a given system (Mishra and Singh, 2010), is still present.

Assumptions that are made in the initial water balance model concept for PDSI are that the top layer of soil holds one inch of moisture, that this moisture is not transferred to the layer beneath until the top layer is completely saturated, that runoff does not occur unless both layers are saturated, and that all of the precipitation that occurs during a month is utilized in that specific month in processes within the water balance model (Heim, 2002). Many have criticized that Palmer's water balance model is too simple to represent the complex hydrological processes that take place. Some of the concerns are the holding capacities of the soil layers remain constant through all seasons, runoff does not occur until both soil layers are saturated, and there is no universal method for calculating evapotranspiration (Alley, 1984). There have been studies that calculate modified versions of PDSI in order to correct for some of the assumptions, however, Palmer's PDSI is still one of the most widely used regional drought indices.

Chapter 3

Methodology

Study Site

The Colorado River Basin (CRB) was selected for this drought study because the basin includes the two largest reservoirs in the U.S. (Lake Mead and Lake Powell) (Kim et al., 2008). These reservoirs "provide municipal and industrial water for nearly 25 million people, agricultural water for 3 million acres, and hydroelectric power for 11.5 billion kilowatt-hours" (Kim et al., 2008). Figure 2 shows the boundaries of the actual Upper and Lower Colorado River Basins, while Figure 3 shows the boundaries of the site for this study.

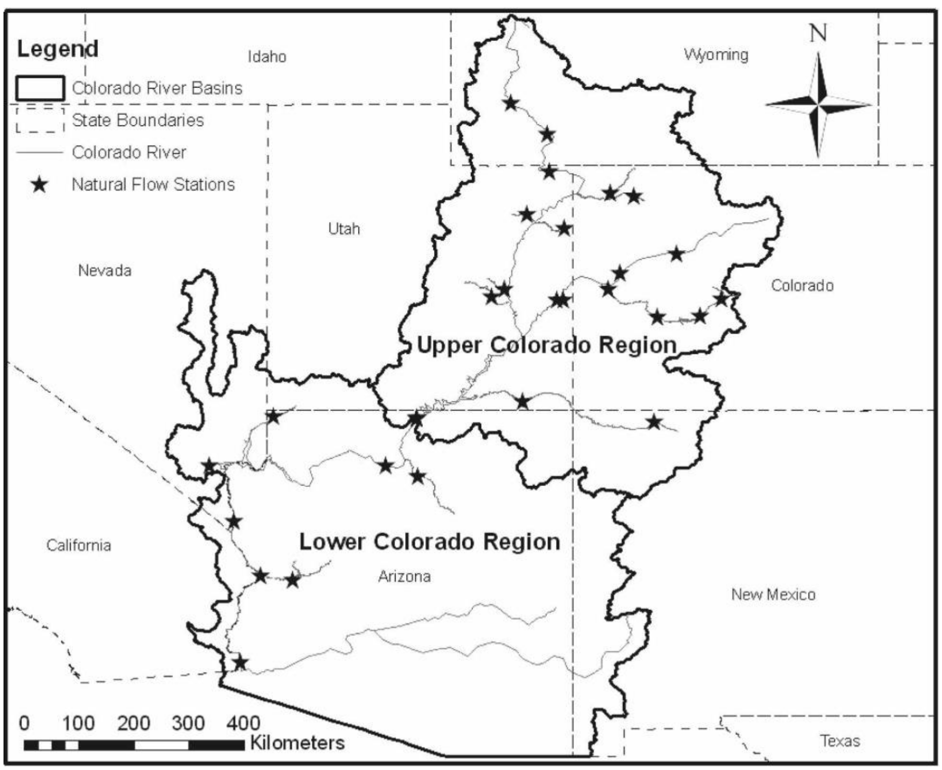

Figure 2. Map delineating the boundaries of the Upper and Lower Colorado River Basins (Miller and Piechota, 2008).

The bounded region in Figure 3 will be referred to as the CRB due to the fact the Upper and Lower CRB represent the majority of the region. Figure 3 also shows the locations of the 437 tree-ring site files and the PDSI grid points that were used in this study.

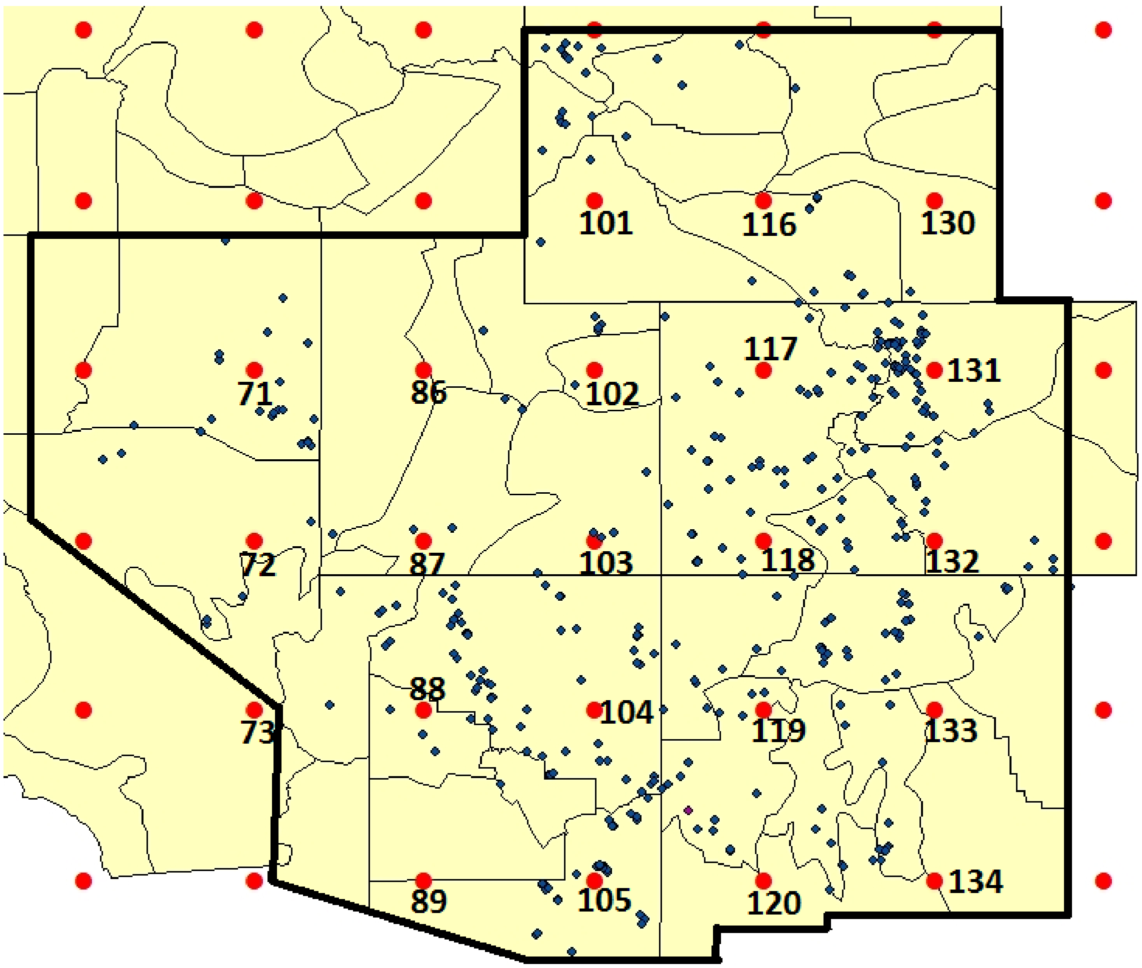

Figure 3. Map showing the Colorado River Basin study site (black boundary). The tree-ring site files (blue diamonds) and PDSI grid points (numbered red dots) used in statistical and spatial analysis are shown as well. Thin black lines within the study region denote climate division boundaries.

This particular boundary was chosen in order to capture the entire CRB, and surrounding areas that could be affected hydrologically. It was also chosen to incorporate the majority of the tree-ring site files that were taken into account by the point-by-point regression (PPR) method used by Cook et al. (1999) to reconstruct PDSI at the indicated grid points. PPR is "the sequential, automated fitting of single-point principal components regression models of tree rings to a grid of climate variables" (Cook et al., 1999). This method is based on the knowledge that drought is a regional phenomenon; therefore, only trees proximal to a particular PDSI grid point are likely to provide information with regard to drought at that location (Cook et al., 1999). For each PDSI grid point, Cook et al. (1999) defined a search radius of 450 kilometers (about 4 degrees latitude/longitude) from which to consider candidate tree-ring predictors of drought for that location. Given that the PDSI grid point spacing is 2.5x2.5 degrees, this means that the PDSI reconstruction is significantly smoothed spatially.

Preprocessing

Raw ring-width and standardized chronology data for 437 site files were downloaded from the International Tree-Ring Data Bank (ITRDB) (ITRDB, 2014). For each site file, multiple raw ring-width core files, and the standardized ring-width index file, were saved as text documents. One site file may contain 50 or more individual raw core files that are stored in the 'Arizona Tree Ring Laboratory' standard format, with measurements in units of 0.01 mm (NCDC, 2014) (Fig. 4). The raw ring-width core text files and the standardized ring-width index text file were imported into Excel to convert raw ring-width data to units of 1.00 millimeter, then imported into the statistics program StatView (SAS institute, 1999) for statistical analysis.

```
061     1 BOBCAT CANYON
061     2 CO, USA       DOUGLAS-FIR        6699  3710N10831W        1390 1971
061     3 DEAN, ROBINSON, BOWDEN
061011  1695   140    36    96    94   109
061011  1700    70   146    50   122    65   122   176    49    75    81
061011  1710    93    78    86    43    30    39    36    42    82    88
061011  1720   171    78    65   131    37   134    96   142    61     8
061011  1730    76    65    75    44   124    16    69    47    68    45
061011  1740    40    55    69   119    87   142   173   212    29   155
061011  1750    67    57    34    55    46    22    45    17    32    37
061011  1760    24    29    35    50    54    29    79    32    81    97
061011  1770    45    90    73     0    58    36    47    50    26    54
```

Figure 4. Example of raw ring-width data format from site file CO076 (Dean et al., 2015).

Figure 4 shows the format of the raw ring-width file. The first three rows contain site-specific information, such as the location name, tree species, latitude and longitude of the site, the earliest and latest year included in the raw data, and the publishing authors. The first column is the site ID, the second column is the first year of each decade, the third column is the raw measurement of the annual ring in units of 0.01 mm for the first year in the decade (1700AD, 1710AD, 1720AD, etc.), the fourth column is the raw measurement of the annual ring in units of 0.01 mm for the second year in the decade (1701AD, 1711AD, 1721AD, etc.), and the pattern continues through the end of the row (NCDC, 2014). Figure 5 shows the format of the standardized ring-width index file.

```
061099 1 BOBCAT CANYON                                           PSME   CO07601   1053 CO07601
061099 2 COLORADO      DOUGLAS FIR       2042M  3710-10831 045 45     1390 1971      CO07601
061099 3 J. S. DEAN, W. J. ROBINSON, D. O. BOWDEN                              07/17/72 CO07601
0610991390 663  11037  11320  11292  11325  11333  1 886  1 792  1 772  1 652  1 CO07601
0610991400 681  1 469  1 638  1 501  11331  1 949  11243  1 948  1 794  11412  1 CO07601
0610991410 951  1 391  11248  1 136  11194  1 593  1 986  11299  1 843  1 720  1 CO07601
06109914201029  2 634  2 941  2 618  21088  21068  21306  21157  21239  21272  2 CO07601
0610991430 819  21099  21358  21103  2 835  2 827  21420  2 921  2 453  2 773  2 CO07601
0610991440 925  21823  2 789  21287  21252  2 736  2 769  2 880  21049  2 824  2 CO07601
0610991450 600  21629  21001  21229  21181  2 292  2 755  2 239  21514  2 951  2 CO07601
0610991460 891  2 603  21110  21231  2 411  2 765  21398  21929  21283  21601  2 CO07601
06109914701301  2 435  2 847  2 541  21023  2 791  21139  21225  21399  2 822  2 CO07601
0610991480 733  2 912  21098  21115  21864  21738  21971  2 972  21388  21848  2 CO07601
06109914901879  22896  21360  21538  21482  2 210  2 859  2 909  21699  21032  2 CO07601
0610991500 125  2 826  21089  21087  21061  2 691  2 292  2 673  2 770  21189  2 CO07601
```

Figure 5. Example of standardized tree-ring index chronology data from site file CO076 (Dean et al., 2015).

The first three rows contain site-specific information, such as the location name, tree species, site elevation, start and end year of the chronology, and publishing authors. For each of the subsequent rows, the first six numbers are the site ID, the next four are the first year of each decade, the next four numbers are the tree-ring index value for the first year of the decade, the next three numbers are how many cores the index measurement is based on, then the pattern continues for each year in the decade (NCDC, 2014). As stated previously, drought conditions are defined to exist for any given year when the index value is less than 1. This definition is based on the process of standardization, where the value 1 indicates the expected growth of a tree in any given year based on its age. Therefore, years with an index value less than 1 tend to be drier with respect to tree growth than those with index values greater than 1.

Statistical Approaches

Using StatView, a Gaussian smoothing filter was designed and used to suppress white noise present in the data. Then, a one-dimensional edge detection filter (Canny, 1986) was applied to the output of the Gaussian smoothing filter to identify years in which rapid changes in ring-width magnitude occurred. This analysis is different from previous studies since the use of the edge detection filter on the tree-ring data in order to identify periods of drought has not been done.

This analysis was applied to all raw ring-width core files, and the standardized ring-width index files. The natural growth function present in the raw ring-width core data was still present in the output of the edge detection filter; therefore, all further analysis was only completed for the standardized chronology index files. Table 1 shows the filter weights associated with both the Gaussian and edge detection filters that were applied to the tree-ring indices. The equations for both the Gaussian and edge filters can be found in Appendix A.

Table 1: Filter Weights					
Filter	**Year – 2**	**Year – 1**	**Year**	**Year + 1**	**Year + 2**
Gaussian	1	2	5	2	1
Edge	n/a	-2	0	2	n/a

Table 1: Weights for both the Gaussian 5-year smoothing filter, and the 3-year moving edge detection filter.

The Gaussian smoothing filter is a 5-year moving filter which increases the signal-to-noise ratio in the data. The edge detection filter is a 3-year moving filter with a step impulse response. Figure 6 shows the index chronology from site file NM529, the output of the Gaussian smoothing filter being applied to the chronology, and the output of the edge detection filter being applied to the output of the Gaussian smoothing filter. The large, positive edge values correspond to a rapid decrease in index value over the 3-year filter period.

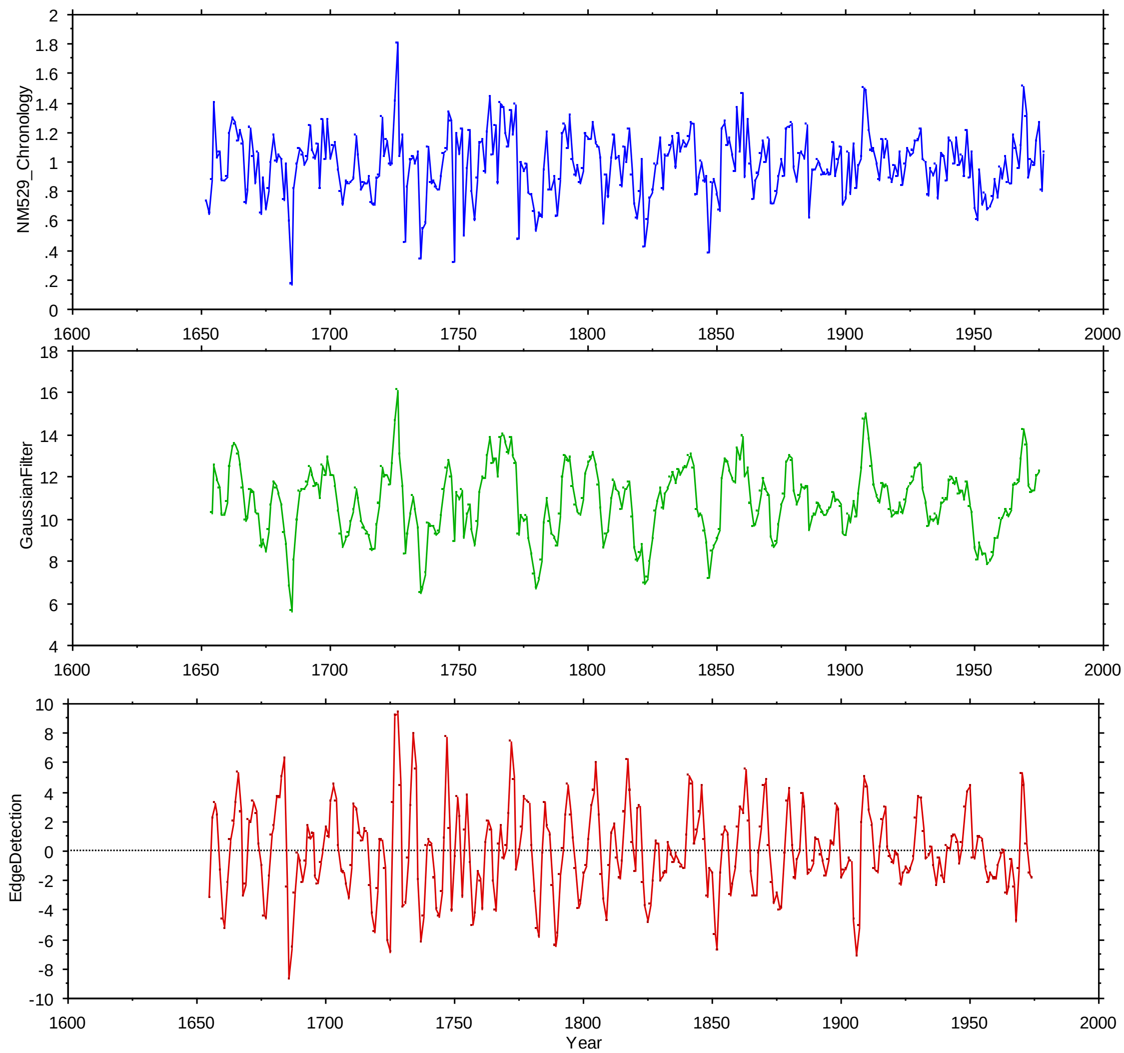

Figure 6. (Top) NM529 site file index chronology. (Middle) Output of Gaussian smoothing filter applied to NM529 index chronology. (Bottom) Output of edge detection filter applied to the output of the Gaussian smoothing filter. Maximums in the edge output that are greater than or equal to 9.1 are considered to be significant because they greater than or equal to 2 standard deviations away from the mean edge value

In this study, reconstructed PDSI from the North American Drought Atlas (Cook and Krusic, 2004) was used as a tool for comparison between the timing of changes in state marked by the edge detection to drought onset marked by the PDSI. To do this, the site files were grouped according to their proximity to a specific PDSI grid point. Table B1 in Appendix B lists the number of site files that were grouped with each PDSI grid point, and the quadrant of which state the PDSI grid point is located. Figure 7 shows the locations of the quadrant boundaries.

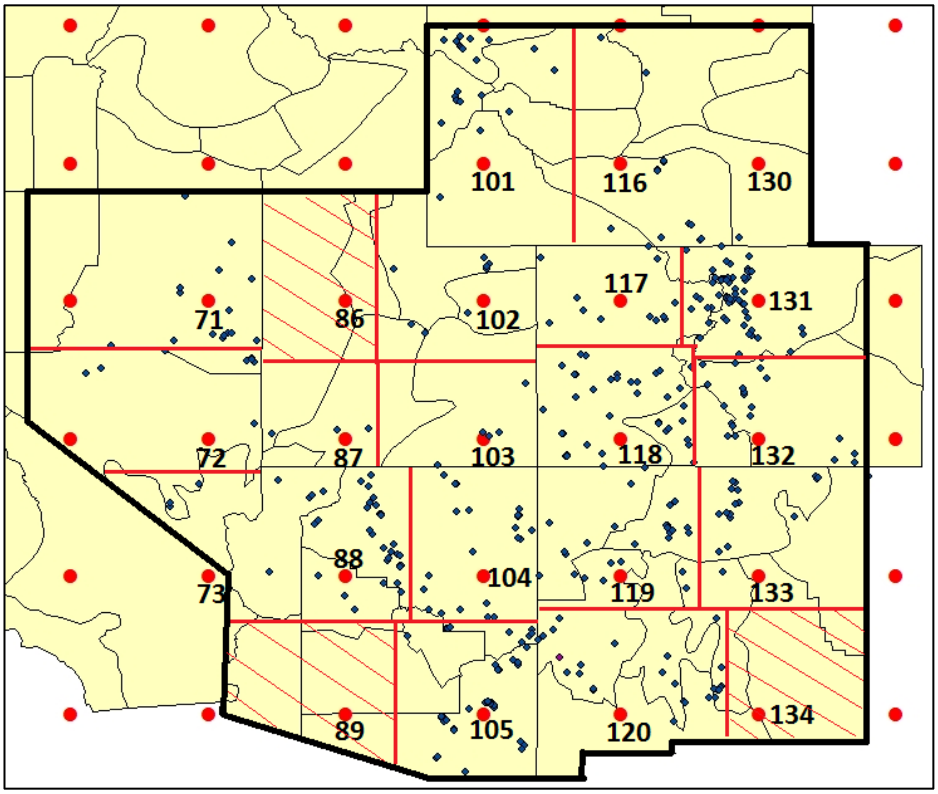

Figure 7. Map of the Colorado River Basin study site (black border), showing the distribution of tree-ring site files (blue dots), and PDSI grid points (red dots). Bold red lines within each state depict quadrant boundaries as they were defined for statistical analysis purposes. Quadrants with diagonal red lines were not used due to the lack of site files in the area.

In order to identify years when a rapid transition to drier conditions occurred in the CRB, three criteria were defined: 1) the presence of a significant positive edge value, 2) a coherent response among the site files, and 3) the significant positive edge must occur in at least 2 quadrants. This drought onset identification was done by transforming the edge detection output for each of the site files within a quadrant to z-scores (subtracting the mean (0.0185) and dividing by the standard deviation (4.641)). Based on the properties of a normal distribution, 95.4% of the data lies within ±2 standard deviations of the mean; therefore, any year when the z-score was greater than +2 was considered to be significant, and corresponds to a change in climatic state (wet to dry). The edge values that correspond to the ± 2 standard deviations away from the mean are 9.3 and -9.2.

Next, the years just prior to the identified significant-edge year were analyzed for coherence, or similar behavior between the site files. This was completed by analyzing each quadrant for instances when the standard deviation between the site file edge output decreased prior to the significant-edge year, signifying a similar response between the site files. Figure 8 shows examples of periods that satisfy criteria 1 and 2 for the Northeast Arizona quadrant.

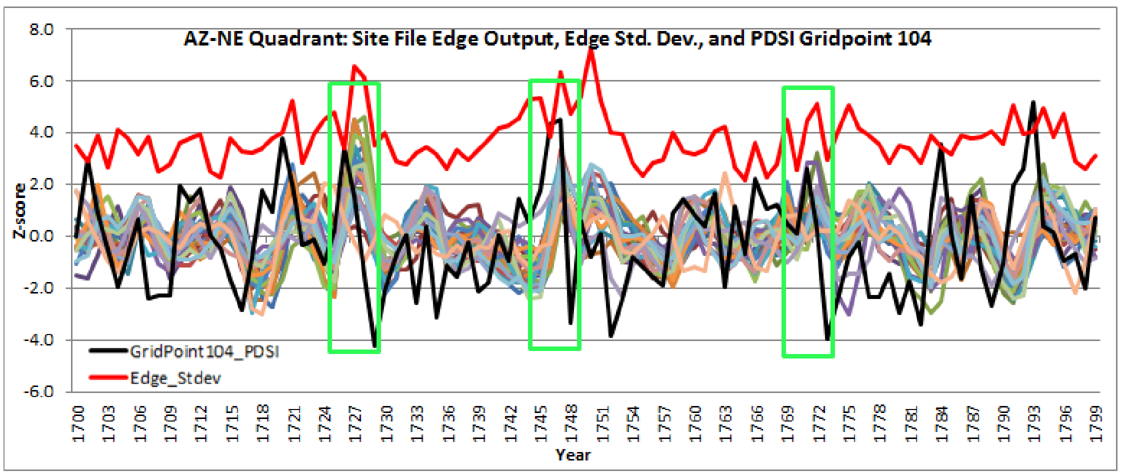

Figure 8. Time series of normalized edge detection output (multi-colored lines) for each site files within the northeast Arizona quadrant, reconstructed PDSI from grid point 104 (black line), and the standard deviation between the edge detection outputs (red line). Time periods highlighted with green boxes satisfy criteria 1 (z-score greater than 2) and criteria 2 (decrease in standard deviation prior to the edge peak).

The following 15 time periods (total of 103 years) listed in Table 2 satisfied all three criteria, and are referred to as the Specified Drought Periods (SDP).

Specified Drought Period	Quadrants
1554AD-1562AD	NM-sw, NM-nw, NM-ne, CO-sw, AZ-ne, AZ-se, NV-east
1610AD-1614AD	NM-sw, NM-nw, AZ-nw, AZ-ne, NV-east, UT-ne
1620AD-1624AD	NM-nw, CO-sw, CO-ne, CO-se, AZ-nw, AZ-ne, AZ-se, NV-east, UT-se
1630AD-1638AD	NV-se, WY-west, NV-east, NV-ne, UT-se
1650AD-1654AD	CO-ne, AZ-nw, UT-se
1680AD-1686AD	NV-sw, NM-nw, CO-nw, CO-ne, CO-se, AZ-nw, AZ-ne, UT-ne
1726AD-1730AD	NM-nw, CO-sw, CO-nw, AZ-nw, AZ-ne, NV-se, NV-east, NV-ne, UT-se, WY-west
1745AD-1749AD	AZ-nw, AZ-se
1771AD-1775AD	NM-nw, AZ-se
1814AD-1820AD	NM-sw, NM-nw, NM-ne, CO-sw, CO-se, AZ-ne, AZ, se
1838AD-1848AD	NM-ne, CO-nw, CO-ne, CO-se, AZ-nw, AZ-ne, AZ-se
1866AD-1872AD	AZ-nw, AZ-ne, NV-east, NV-ne, UT-ne, WY-west
1876AD-1882AD	CO-ne, CO-se
1930AD-1936AD	NM-sw, AZ-se, NV-se, NV-east, WY-west, WY-cen/east
1948AD-1956AD	NM-se, NM-nw, NM-ne, CO-sw, CO-ne, CO-se

Table 2. Quadrants that experienced drought onset (z-score greater than or equal to 2) during specified drought periods.

A SDP was determined to end when there was a negative edge peak, signaling a transition from dry to wet conditions. All further analysis was performed only for these SDPs.

Within each SDP, a peak drought index and edge year was identified. The index values for all site files were averaged for each year during each SDP. The year that had the lowest index average within each SDP was designated as the peak index drought year. Next, the edge detection values for all of the site files were averaged for each year during each SDP. The year that had the highest edge average within each SDP was designated as the peak edge year. Because a large positive edge value for year ‘x’ indicates a sudden decrease in index value from year ‘x-1’ to year ‘x+1’ it is expected that the peak edge year would occur before the peak index drought year. Table B2 in Appendix B lists the peak index year and peak edge year for each SDP.

GIS Approaches

Two separate StatView files were created, one with the index chronologies for all 437 site files, and one with the edge detection output for all 437 site files. Each StatView file was then transposed into Excel so that individual rows consisted of a separate site file. Prior to the year 1500AD and post 1960AD, the majority of the site files have fewer tree-ring index values. For this reason, analysis of index and edge detection data was limited to 1500AD-1960AD. The index and edge detection Excel files were then imported into ArcMap, each separated into 100-year increments due to program limitations (Index 1500AD-1599AD, Edge 1500AD-1599AD, Index 1600AD-1699AD, Edge 1600AD-1699AD, etc.). For each 100-year index and edge file, any site file that did not have a complete record for that time period was discarded. This was done because ArcMap automatically replaces blank spaces within text files with the value of zero upon converting the text file to a shapefile. In the case of tree-ring index measurements, a value of zero indicates a year of no growth, as opposed to a blank space which would indicate that there is not an index measurement for that particular year. This modified dataset is referred to as the “trimmed” dataset, and it was used for all spatial analysis. Table B3 in Appendix B shows the number of site files that were used for each 100-year period.

The Inverse Distance Weighting (IDW) tool was used to create maps of index values and edge detection values for each year from 1500AD-1960AD for the entire CRB region. IDW interpolation assumes that points that are closer together are more alike than those that are farther apart ($ArcGIS_1$, 2012). To assign an index or edge value to an unmeasured location, “IDW assumes that each measured point has a local influence that diminishes with distance,” therefore it gives more weight to the measured index and edge values that are closest to the prediction location and the weights diminish as a function of distance ($ArcGIS_1$, 2012). Drawbacks to IDW interpolation are that it is an exact interpolator, so the maximum and minimum index and edge values can only occur at measured locations, even though this may not actually be the case ($ArcGIS_1$, 2012). IDW interpolation is also sensitive to clustering of measured locations and outliers ($ArcGIS_1$, 2012).

Another spatial analysis tool available in ArcMap used for interpolation is kriging. Kriging approaches have the assumption that some of the spatial variance between the locations of measured index values can be modeled by random processes with spatial autocorrelation, where the spatial autocorrelation model must be known (ArcGIS, 2013). Kriging was not used in this case because of the lack of information to explicitly model the spatial autocorrelation associated with the random processes that affect the index values, however with more information in the future this may be an appropriate interpolator for the dataset.

Once the specified drought periods were selected from the results of the statistical analysis, the corresponding index maps for each year within the time periods were combined for a Principal Components Analysis (PCA) (the same was done for the edge detection maps). PCA is a way of identifying patterns in data, and expressing the data in a way that highlights the similarities and differences (Smith, 2002). PCA is the transformation of data into a new multivariate attribute space, where the axes of the new space are rotated with respect to the old space ($ArcGIS_2$, 2012; Smith, 2002). In other words, the axes are rotated in order to best fit the variance of the data. The new, rotated axes are known as eigenvectors, and their length is described by an eigenvalue. Eigenvectors are the “axes” (directions) along which a linear transformation occurs by “stretching/compressing” and/or “flipping”; eigenvalues give you the factors by which this stretching/compressing occurs. The eigenvector with the largest eigenvalue is known as the first principal component. It captures the most significant relationship between the data, and explains the largest portion of variance within the dataset ($ArcGIS_2$, 2012; Smith, 2002). In this case, mapping the first principal component (PC1) loadings will produce a map of the spatial pattern that explains the greatest amount of variance within the index data during SDPs. The eigenvector with the second largest eigenvalue (PC2) is aligned such that it captures the maximum remaining variance in the dataset (explaining the second-highest amount of variance within the data) ($ArcGIS_2$, 2012; Smith, 2002). Mapping PC2 loadings produces a map of the spatial pattern that explains the next highest amount of variance not explained by the first. In many cases, more than 90% of the variance can be explained by the first three eigenvalues (Smith, 2002).

Chapter 4

Data Analysis

Edge Detection

The output of the Gaussian smoothing and edge detection filters was previously shown in Figure 6, but a closer look at the edge output versus the index chronology is presented in Figure 9 below. The normalized index and edge output for site file NM030 are shown from 1700AD-1749AD.

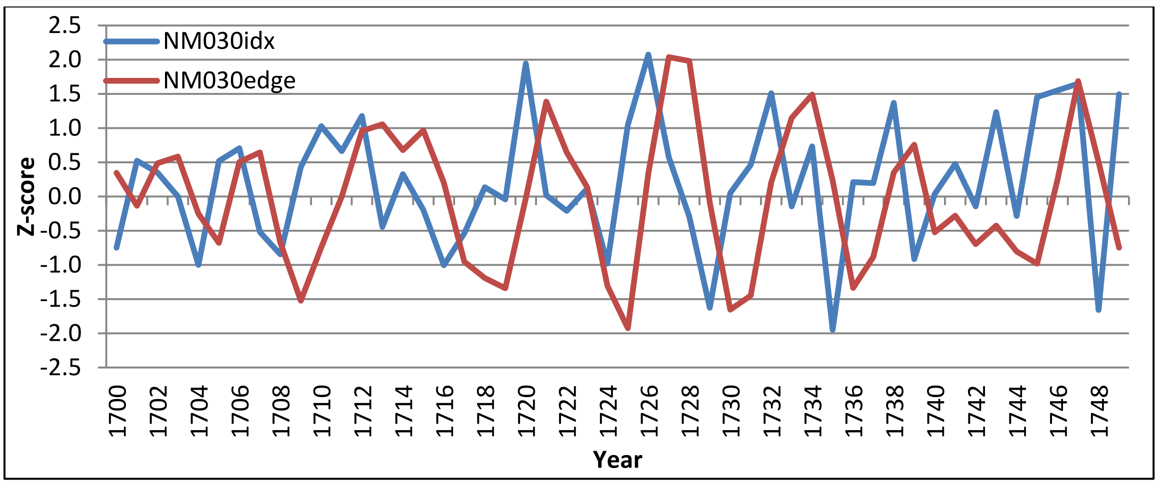

Figure 9. Normalized index (blue) and edge output (red) for site file NM030 from 1700AD-1749AD.

The index value reaches a maximum in the year 1726AD and begins to decrease until it reaches a minimum in 1729AD. The maximum edge value occurs during the years of the transition from the maximum index value to the minimum index value (1727AD and 1728AD). This large, positive edge value marks a change in state from relatively wet conditions to relatively dry conditions. Mapping the edge response shows which sites are experiencing transitions from relatively wet (high index value) to relatively dry (low index value) conditions, based on the sites experiencing significant positive edge values.

Figures 10a and 10b show the IDW spatial interpolation of the index and edge values for the year 1561AD, respectively.

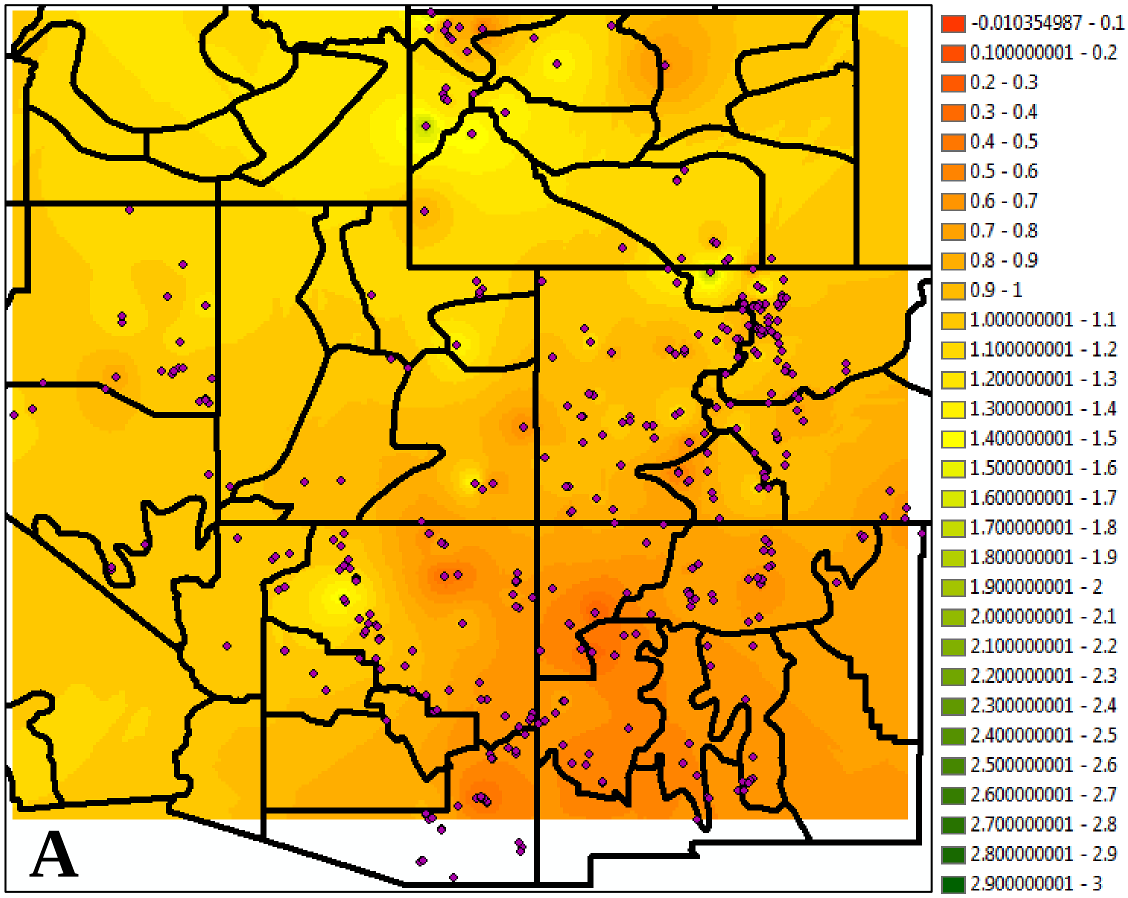

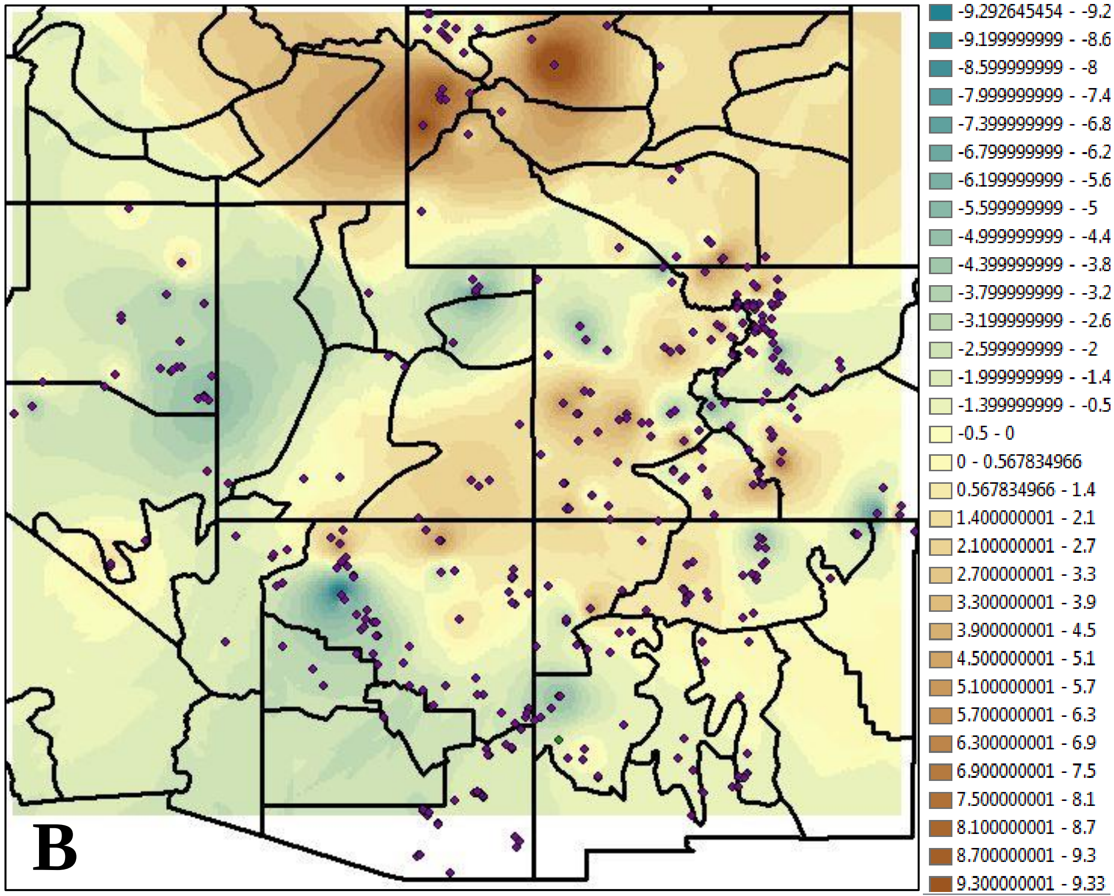

Figure 10. (a) Map of the IDW spatial interpolation of the index values for the year 1561AD, (b) Map of the IDW spatial interpolation of the edge values for the year 1561AD. Climate division boundaries (black lines) and all 437 site files (purple dots) are shown.

In Figure 10a, red and orange areas experienced relatively dry conditions (index values less than 1), while yellow and green areas experienced relatively wet conditions (index values greater than or equal to 1). In Figure 10b, areas shaded blue experienced negative edge values, indicating a transition from a relatively low index value to a relatively high index value (dry to wet conditions). Areas shaded brown experienced positive edge values, indicating a transition from a relatively high index value to a relatively low index value (wet to dry conditions). The maximum and minimum edge values on the color bar are the significant edge values located ±2 standard deviations away from the mean. If any site file experiences an edge value outside of these bounds, the site file will be assigned either -9.2 or 9.3 (depending on the transition type).

Analyzing the sequence of IDW edge interpolation maps for each SDP allows for the identification of edge migration patterns. Figure 11 (a-e) shows the edge and index IDW interpolation maps from 1726AD to 1730AD.

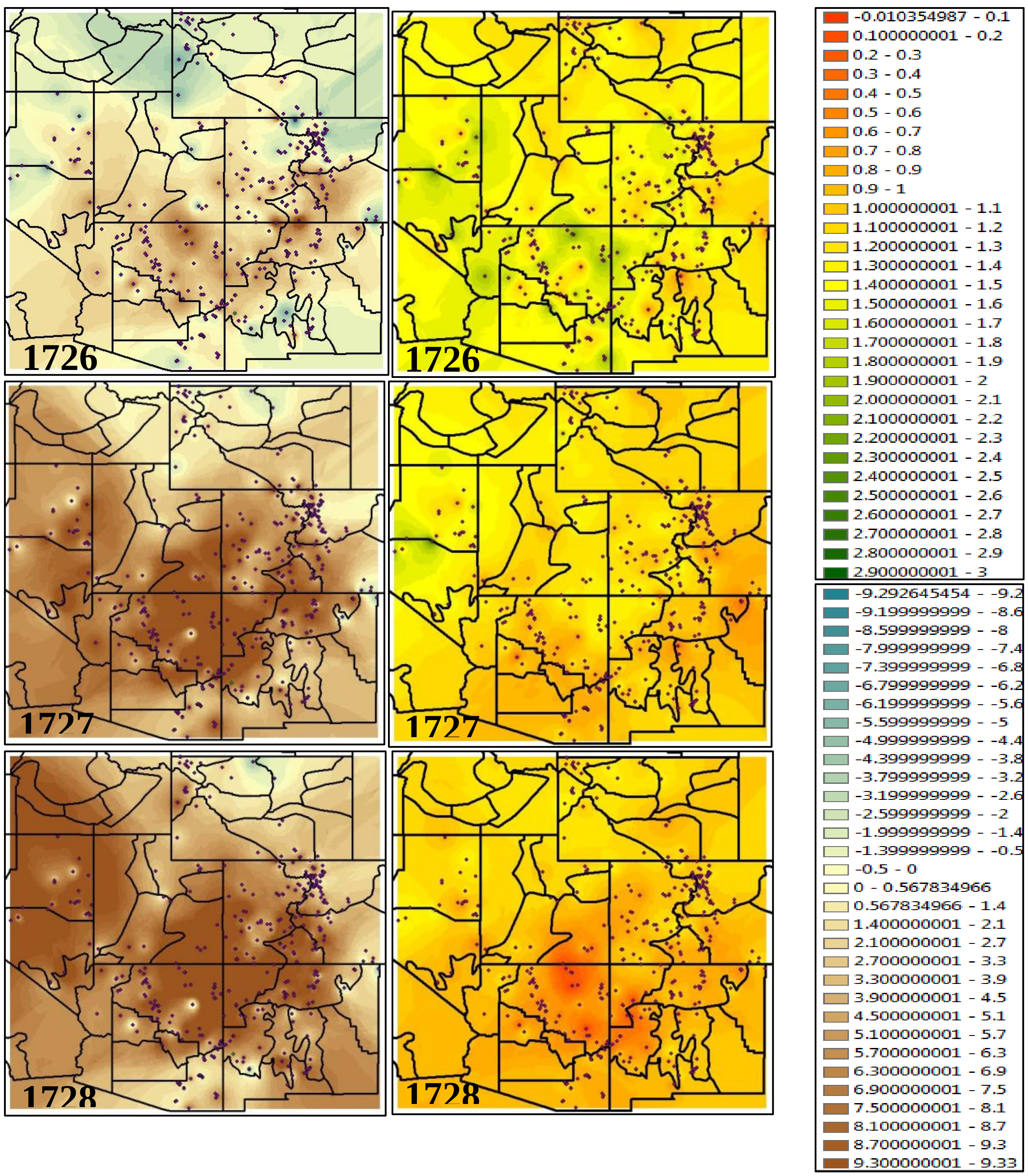

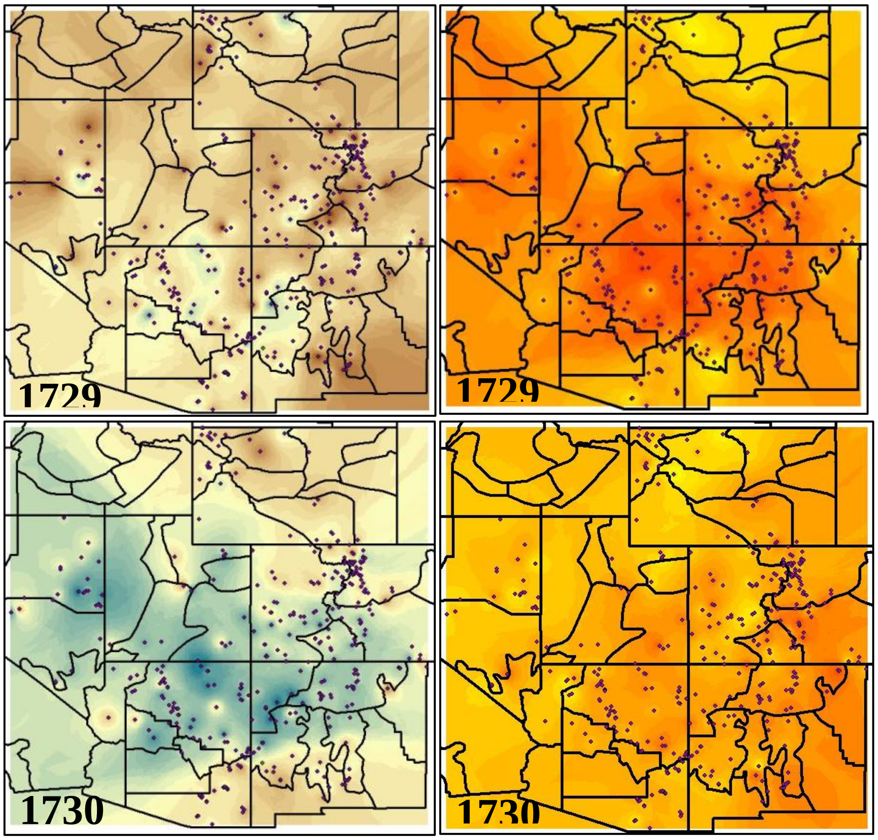

Figure 11. IDW edge (left) and index (right) interpolation for 1726AD to 1730AD. Purple diamonds show the locations of each site file.

In 1726AD (Fig. 11a), the edge detection (left) indicates site files on the border between New Mexico and Colorado, and also on the border between Arizona and Utah, experienced positive edge values, meaning these are the locations experiencing a transition from relatively high to relatively low index values (wet to dry conditions). In 1727AD (Fig. 11b, left), the positive edge values intensified and expanded to site files within the Four Corners region, and in portions of eastern Nevada. Further intensification occurred in 1728AD (Fig. 11c, left), where site files in northeastern Nevada and northwest Colorado experienced larger positive edge values. Within this time period, 1728AD is the peak edge year (experienced the most positive edge values), which indicates that the greatest decrease in index magnitude (rapid change of state) took place from 1727AD to 1729AD. The edge detection for 1730AD (Fig. 11e, left) shows many of the site files transitioning to negative edge values, indicating a change to relatively larger index values (wetter conditions). Figure 12(a-i) shows the edge migration for the SDP 1948AD to 1956AD.

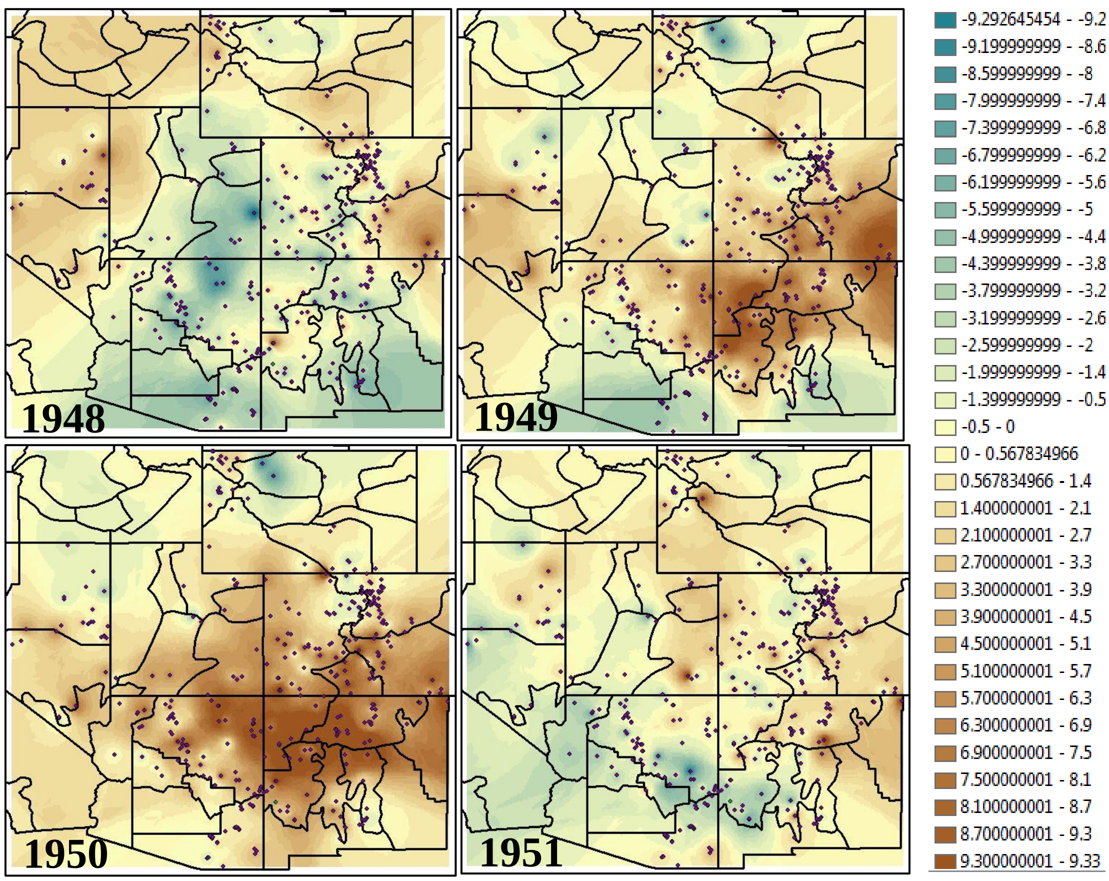

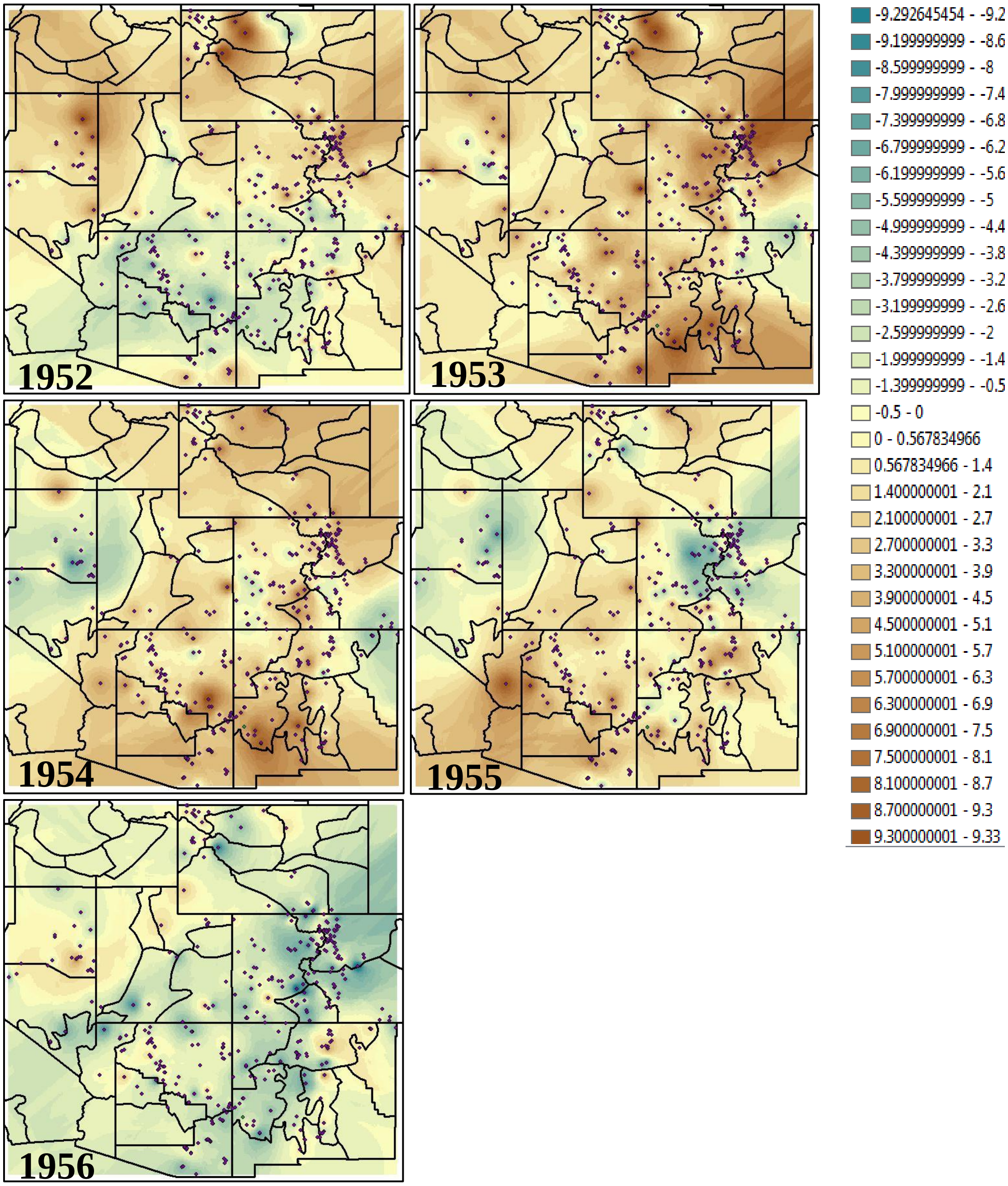

Figure 12. IDW edge detection interpolation maps for 1948AD through 1956AD. Black lines represent climate division boundaries, and purple dots show the site file locations. The dark brown areas represent significant positive edge values, and show drought onset.

Analyzing the edge migration/intensification pattern for each SDP will allow for the identification of any similarities between the onset and termination of droughts.

Principal Components Analysis

A Principal Components Analysis (PCA) was performed in the Spatial Analyst extension of ArcMap on the index and edge maps of the SDPs in order to highlight the statistical patterns between the site files. Figure 13 below shows the 3 principal components (PCs) for the index data, along with the amount of variance explained by each.

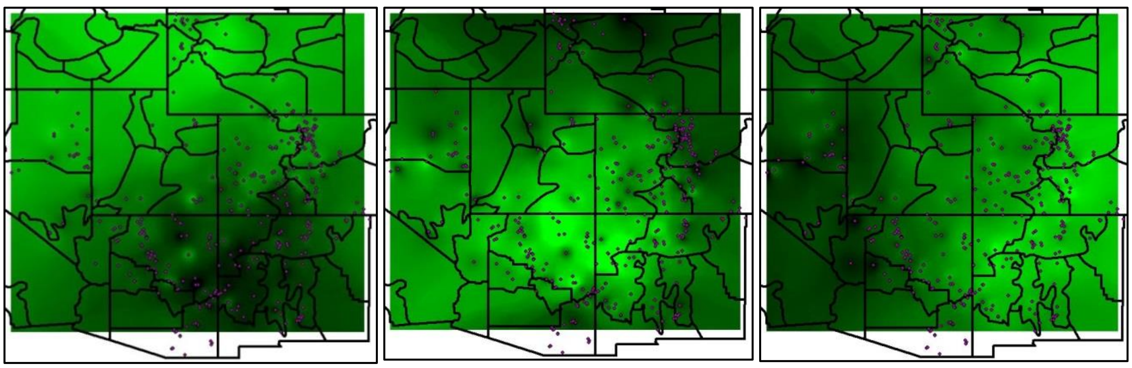

(47%) (37%) (16%)

Figure 13. Principal components analysis of the site file index data. (Left) PC1, explaining 47% of the variance. (Middle) PC2, explaining 37% of the variance. (Right) PC3, explaining 16% of the variance. Site files included in the analysis are shown as purple dots.

PC1 (Fig. 13, left) explains 47% of the variance of the index data, and shows a significant divide between the northern and southern portions of the CRB, with negative loadings over the southern Rockies, northwestern New Mexico, and east-central Arizona. PC2 (Fig. 13, middle) explains 37% of the variance, with positive loadings centered on the Four Corners region (central CRB). PC3 explains 16% of the variance within the index data, and exhibits an east-west divide pattern where the sites in the eastern portion of the CRB have positive loading values while western Arizona and Nevada sites have negative values.

Figure 14 shows the 3 PC maps of the edge detection data for all of the SDPs.

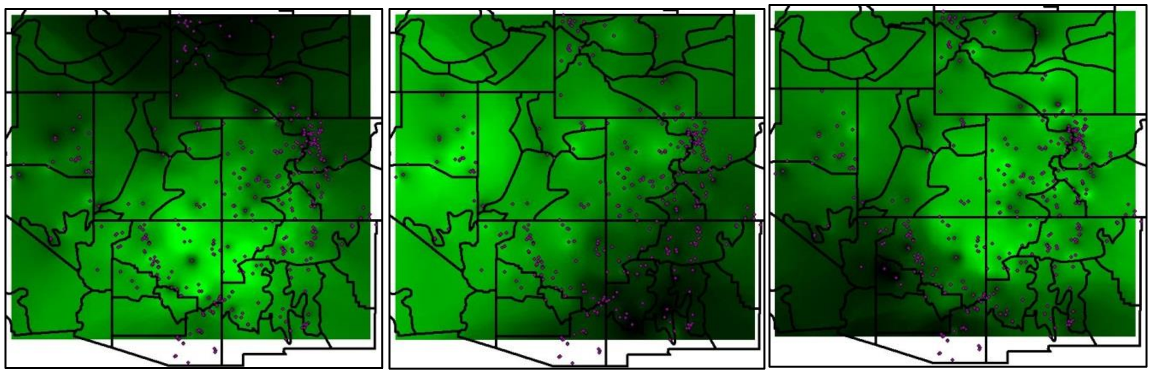

(60%) (27%) (13%)

Figure 14. Principal components analysis of the site file edge detection data. (Left) PC1, explaining 60% of the variance. (Middle) PC2, explaining 27% of the variance. (Right) PC3, explaining 13% of the variance. Site files included in the analysis are shown as purple dots.

PC1 (Fig. 14, left) explains 60% of the variance of the edge detection data. The site files in the Four Corners region (central CRB) and the southern portion of the CRB have positive loadings while the site files in Wyoming have negative loadings. PC2 (Fig. 14, middle) explains 27% of the variance, and the sites with positive loadings located in eastern Nevada, northern Arizona, and northwest Colorado, while sites in New Mexico have negative loadings. PC3 explains 13% of the variance the edge detection data, with sites located in the Four Corners region (central CRB) and the eastern half of the CRB (northern New Mexico, Colorado, and central/eastern Wyoming) having positive loadings, and sites in southern New Mexico and most of Arizona have negative loadings.

A PCA was also completed for only the peak edge years within each SDP. The results are shown in Figure 15.

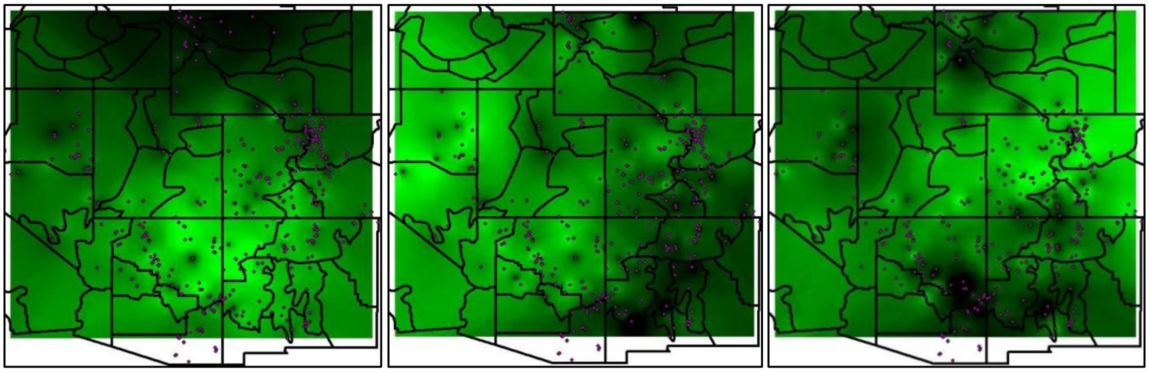

Figure 15. Principal components analysis of the site file edge detection data for the peak edge years within each SDP. (Left) PC1, explaining 75% of the variance. (Middle) PC2, explaining 16% of the variance. (Right) PC3, explaining 9% of the variance. Site files included in the analysis are shown as purple dots.

Given that these peak edge years were taken into account for the PCA analysis shown in Figure 14, it is expected that the PC maps in Figure 15 would look similar to those in Figure 14, respectively. However, there are some subtle differences which are expressed in the different values of variance explained by each PC.

A sampling uncertainty test, as outlined by North et al. (1982), was completed for each PCA to determine if each PC pattern was representative of the true pattern. The sampling error calculation is shown in Equation 3.

$$\delta\lambda_i = \lambda_i * \left(\frac{2}{\nu}\right)^{\frac{1}{2}} \tag{3}$$

In equation 3, λ represents each eigenvalue and ν represents the degrees of freedom, where the degrees of freedom is equal to the number of sampling points (103 years for the Index and Edge PCA, 15 years for the Peak Edge Year PCA). The results of the sampling error calculation are shown in Table 3.

PCA Type	λ1	δλ1	λ1 Range	λ2	δλ2	λ2 Range	λ3	δλ3	λ3 Range
Index	1.31	±0.18	1.49-1.13	1.01	±0.14	1.15-0.87	0.45	±0.06	0.51-0.39
Edge	233	±32	265 - 201	104	±14	118 - 90	52	±7	59 - 45
Peak Edge Year	86	±31	117 - 54	18	±7	25 - 11	10	±4	14 - 6

Table 3. Eigenvalues (λ), sampling error in the eigenvalue (δλ), and the sampling error envelope (λ range) for the eigenvalue for each PCA type.

It has been shown that each PC pattern is sufficiently independent of the surrounding PC patterns if the sampling error envelope does not overlap with the eigenvalue of the surround PC (North et al., 1982). In this study, each PC pattern is sufficiently independent, and is therefore able to be interpreted as representing the true pattern.

Superposed Epoch Analysis

A Superposed Epoch Analysis (SEA) was completed to determine if there were similarities in the timing of the edge detection between the SDPs. This type of analysis is used to characterize a “response” index for a single type of event (Haurwitz and Brier, 1981). For each SDP, the edge values of the site files within the quadrants that exhibited a significant edge during that period were averaged for each year of the SDP. The SDP edge averages were plotted for an 8-year period (initiation year 0, through ending year 8). This type of comparison is designed to illustrate any response that is locked in time, rather than specific to any individual event (Haurwitz and Brier, 1981). In this case, if each SDP has a similar edge response, this will be evident in the analysis. Figure 16 shows the results of the SEA.

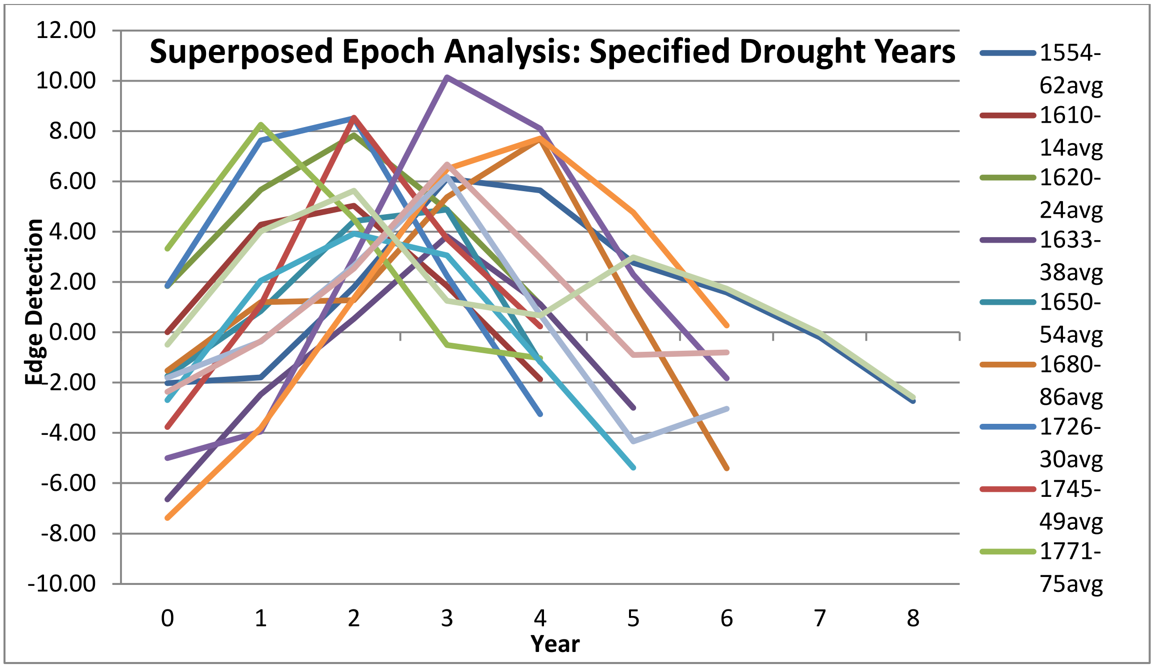

Figure 16. Superposed Epoch Analysis of the average edge response for each of the specified drought periods.

Each of the SDP edge averages exhibit an increase in edge value from year 0 to year 2. After year 2, some of the averages begin to decrease while others continue to increase and peak in either year 3 or 4. Table 4 shows which SDPs peak in year 1 or 2 versus the SDPs that peak in year 3 or 4.

Year of Edge Peak	Specified Drought Periods
1 or 2	1610AD-1614AD, 1620AD-1624AD, 1650AD-1654AD, 1726AD-1730AD, 1745AD-1749AD, 1771AD-1775AD, and 1843AD-1848AD
3 or 4	1554AD-1562AD, 1633AD-1638AD, 1680AD-1686AD, 1814AD-1820AD, 1866AD-1872AD, 1876AD-1882AD, and 1930AD-1936AD

Table 4. List of SDPs and which years in the Superposed Epoch Analysis that the edge peak occurs.

To determine whether the edge trends illustrated in Figure 16 were a part of a pattern, or simply random, a separate SEA was conducted. Between 1500AD and 1960AD, 15 random time periods were selected that did not include any of the years in the SDPs, but that did include the same total number of years as are in the analysis in Figure 16. The results are shown in Figure 17.

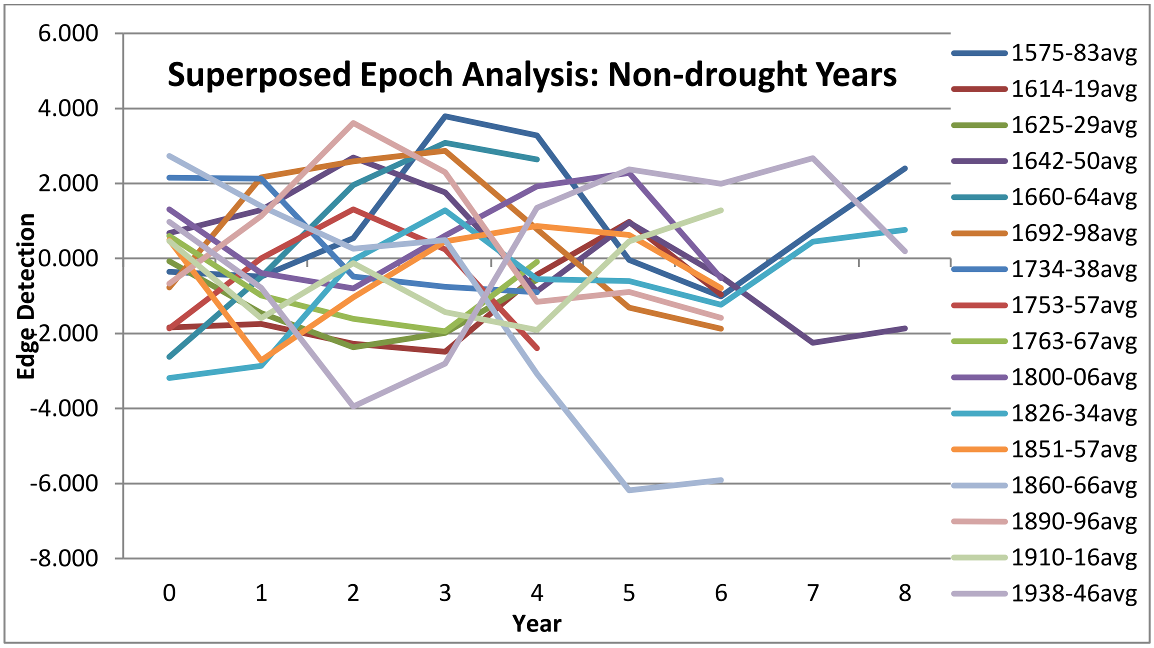

Figure 17. Superposed Epoch Analysis of the average edge response of 15 random "non-drought" periods.

This SEA suggests that there is no apparent trend between the non-drought edge averages, which further supports the existence of a pattern between the SDP edge averages.

Differences in Species Sensitivity

In order to determine if there are large differences in ring-width index based on the species of tree, time series of the average index for each species were made for each SDP. Only species that appeared in more than 2 out of the 6 states in the CRB were used, to ensure a wide coverage. The results for the 1680AD-1686AD and 1745AD-1749AD SDPs are shown in Figure 18(a-b).

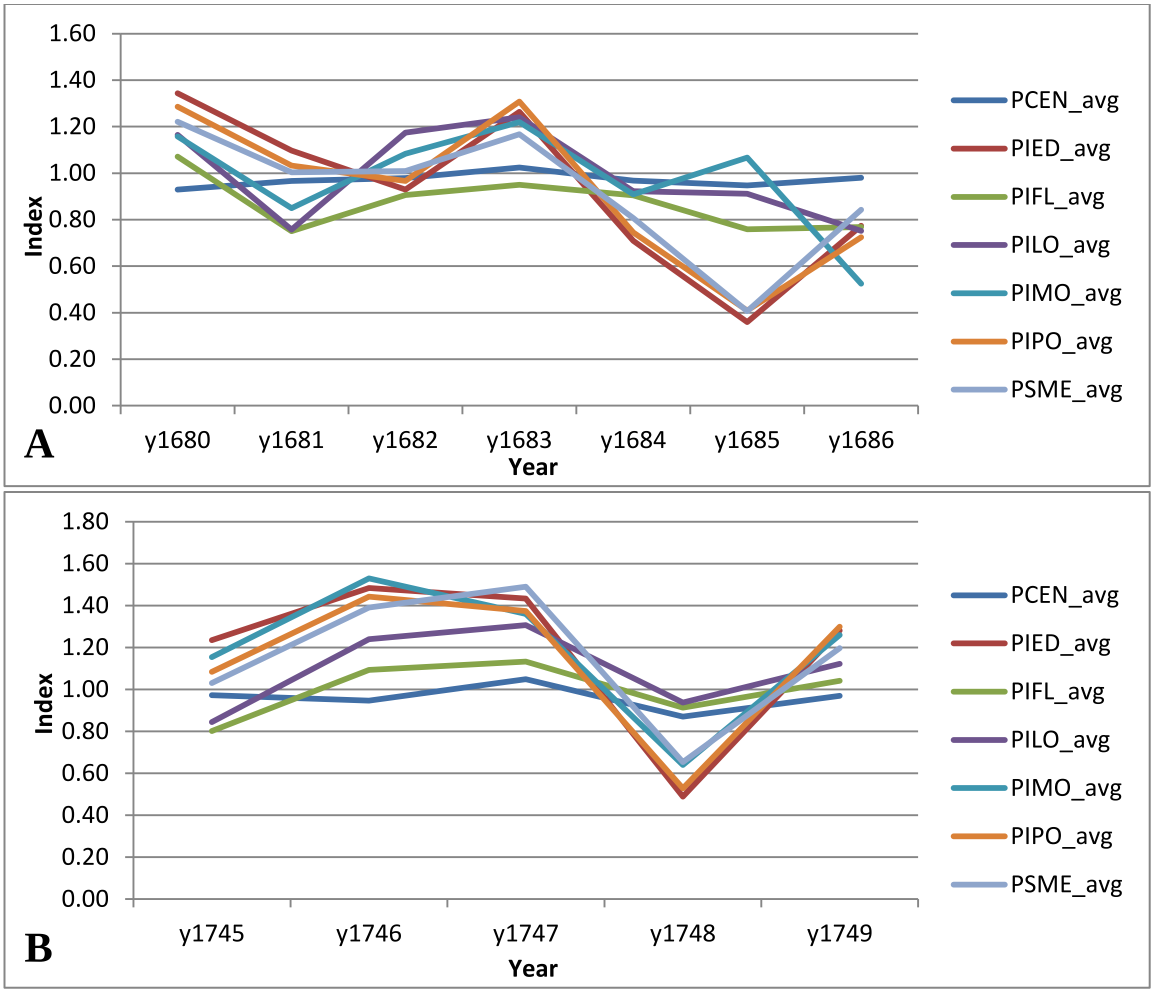

Figure 18. (a) Species-averaged index for 1680AD-1686AD. (b) Species-averaged index for 1745AD-1749AD.

It is a common feature in all 15 SDPs that the PILO, PIFL, and PCEN species were less sensitive to changes in state than PIED, PIMO, PIPO, and PSME (see Table B4 in Appendix B for tree species codes). The species that had common trends in sensitivity were then averaged together. Figure 19(a-e) shows the results. Years in which all of the species displayed an equal sensitivity to a change in state are 1632AD (Fig. 19b), 1819AD (Fig. 19d), 1842 (Fig. 19d), and 1934AD (Fig. 19e), suggesting that the shift from wet to dry conditions during these respective SDPs was of greater magnitude.

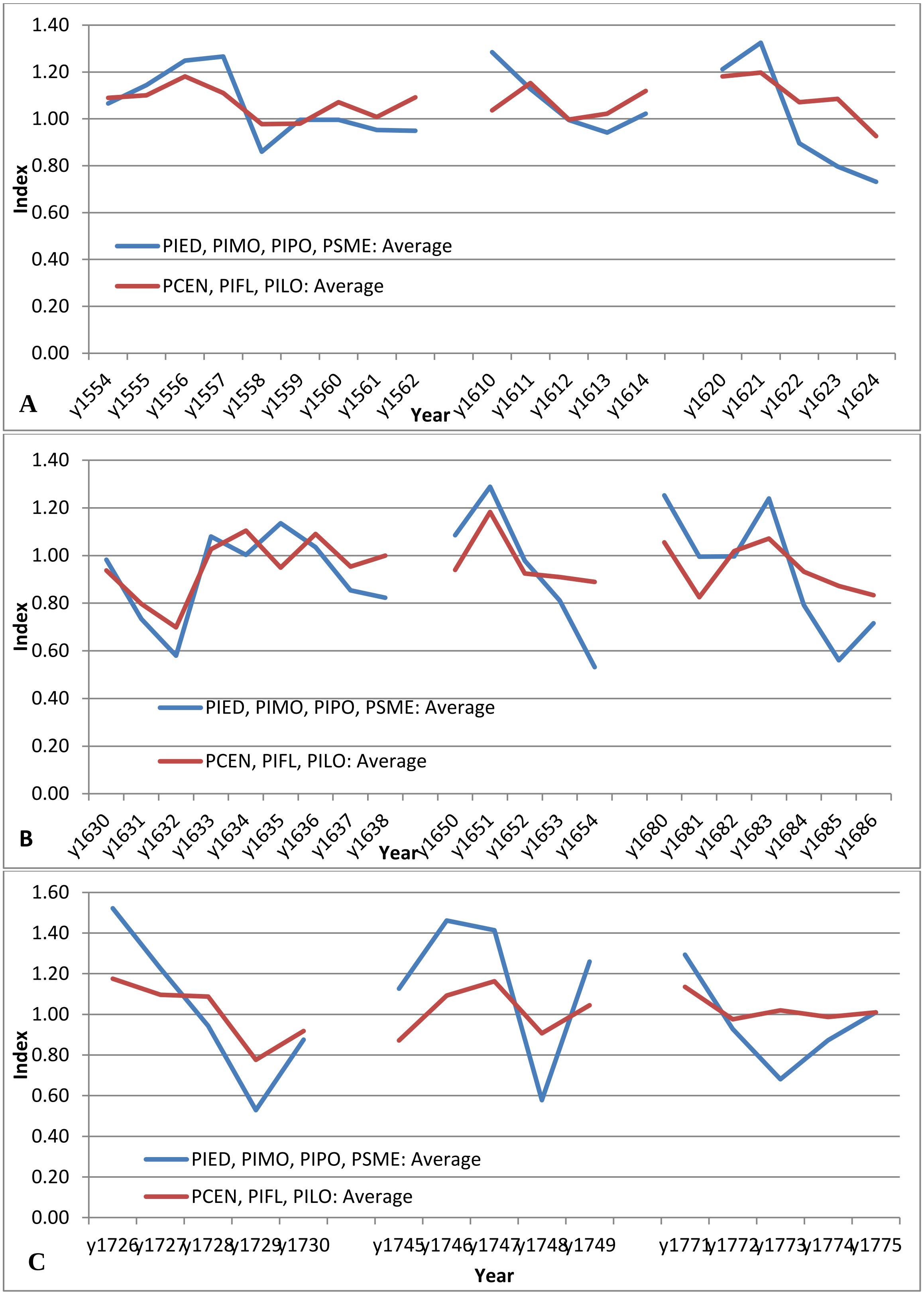

A
Index
1.40
1.20
1.00
0.80
0.60
0.40
0.20
0.00
PIED, PIMO, PIPO, PSME: Average
PCEN, PIFL, PILO: Average
y1554 y1555 y1556 y1557 y1558 y1559 y1560 y1561 y1562
y1610 y1611 y1612 y1613 y1614
y1620 y1621 y1622 y1623 y1624
Year
B
Index
1.40
1.20
1.00
0.80
0.60
0.40
0.20
0.00
PIED, PIMO, PIPO, PSME: Average
PCEN, PIFL, PILO: Average
y1630 y1631 y1632 y1633 y1634 y1635 y1636 y1637 y1638
y1650 y1651 y1652 y1653 y1654
y1680 y1681 y1682 y1683 y1684 y1685 y1686
Year
C
Index
1.60
1.40
1.20
1.00
0.80
0.60
0.40
0.20
0.00
PIED, PIMO, PIPO, PSME: Average
PCEN, PIFL, PILO: Average
y1726 y1727 y1728 y1729 y1730
y1745 y1746 y1747 y1748 y1749
y1771 y1772 y1773 y1774 y1775
Year

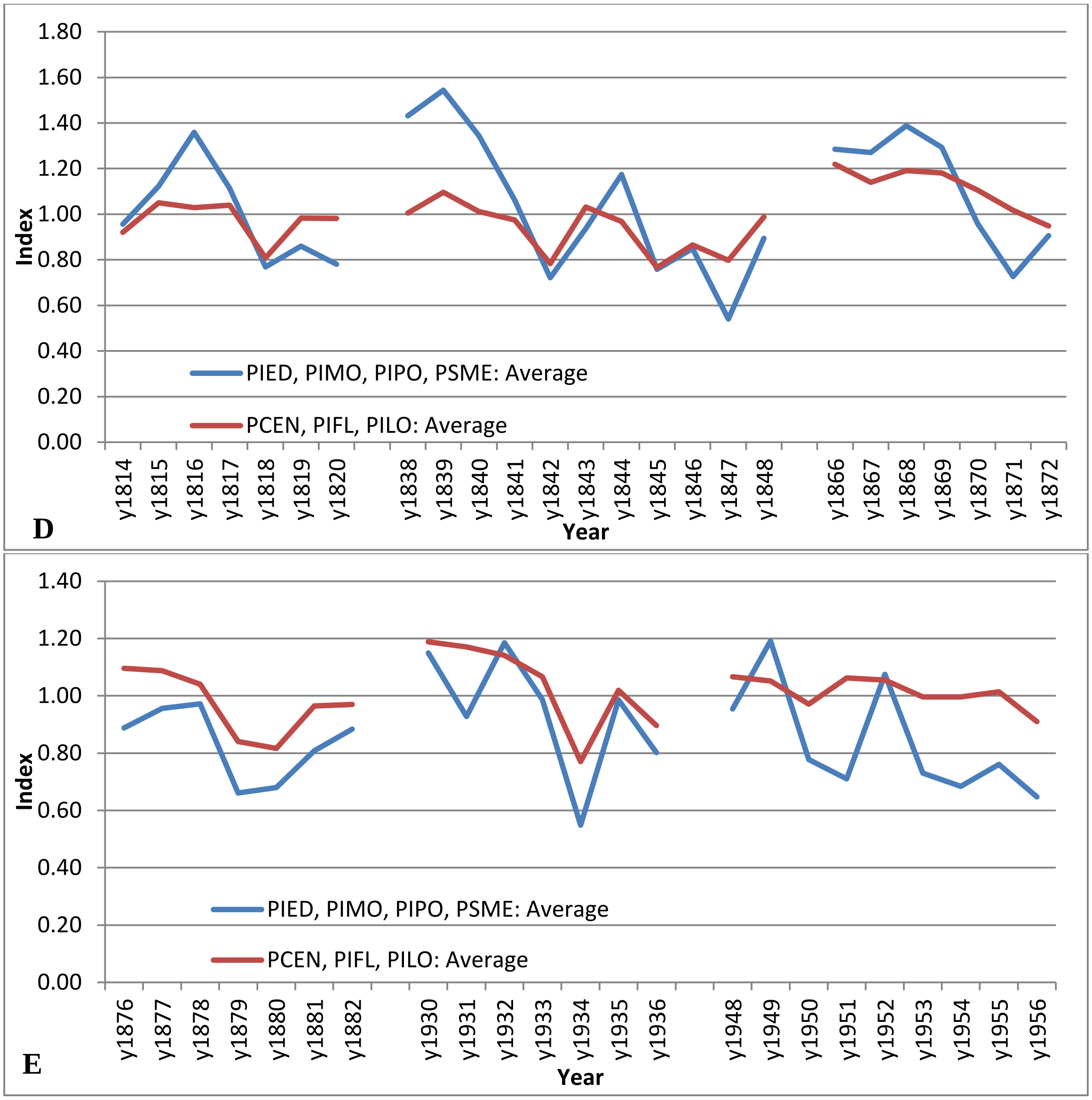

Figure 19(a-e). Precipitation-sensitive species index values (blue line), and temperature-sensitive species index values (red line) for each specified drought period. The temperature-sensitive species index values are generally more stable than the precipitation-sensitive species. Years where both precipitation- and temperature-sensitive species exhibit equal sensitivity to changes in state (wet to dry) are 1632AD (b), 1819AD (d), 1842AD (d), and 1934AD (e).

Chapter 5

Interpretations

Assessing the Edge Detection filter

To assess whether the edge detection filter was successful in identifying the onset of changes of state from wet to dry, the edge detection output for each quadrant was compared to reconstructed PDSI from the respective PDSI grid point (Table B1, Appendix B). Figure 20(a-c) shows the edge detection output for three different quadrants compared to the reconstructed PDSI for their respective grid points.

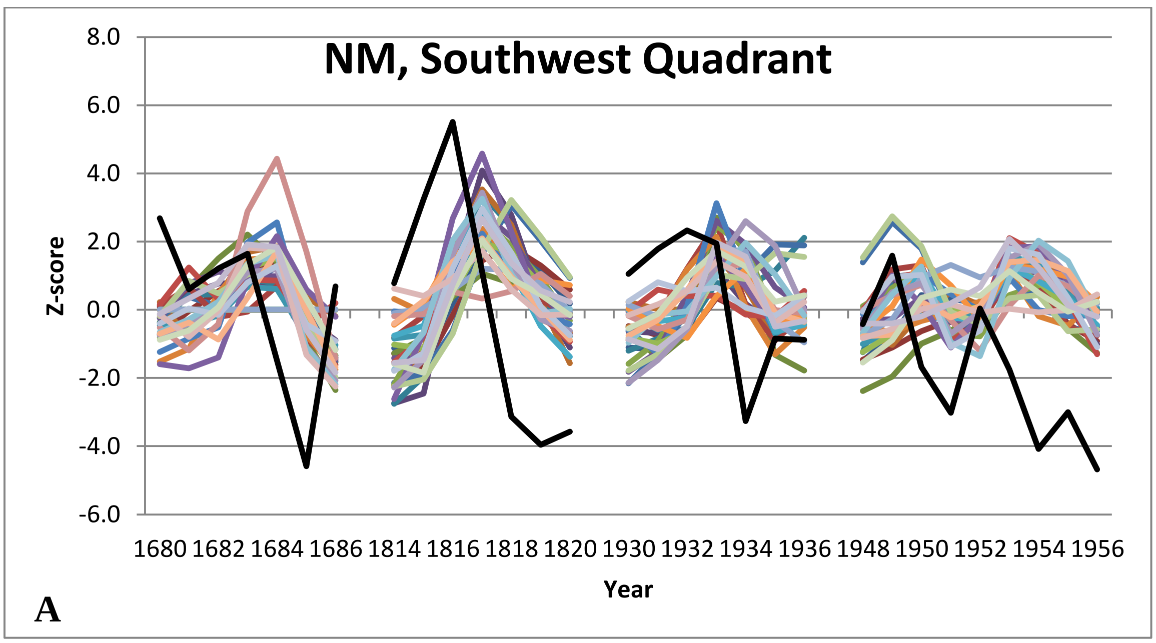

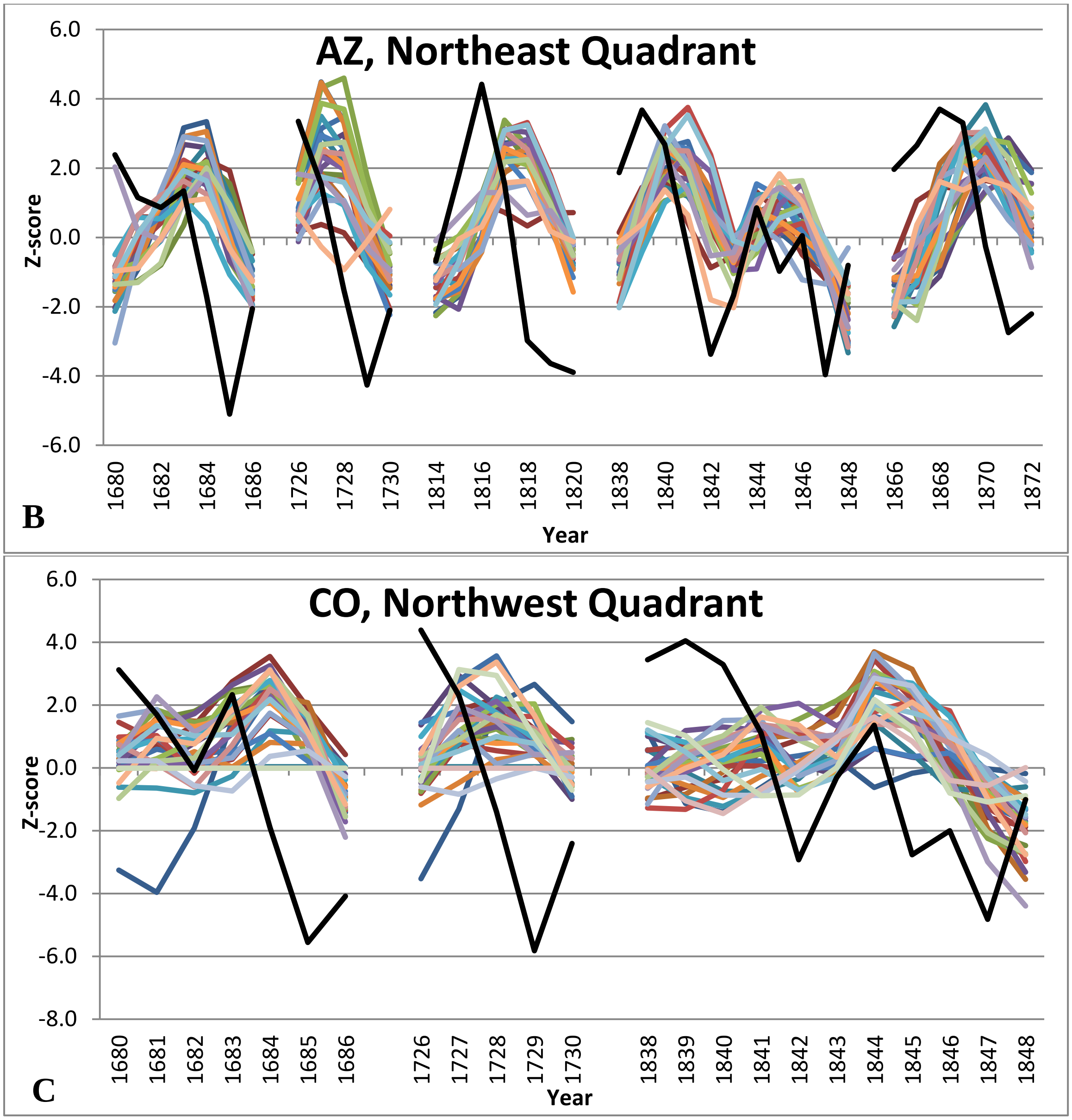

Figure 20(a-c). (a) Normalized edge output from site files in the New Mexico southwest quadrant (colored lines) and reconstructed PDSI from grid point 120 (black line) for SDPs identified for that quadrant. (b) Normalized edge output from site files in the Arizona northeast quadrant (colored lines) and reconstructed PDSI from grid point 104 (black line) for SDPs identified for that quadrant. (c) Normalized edge output from site files in the Colorado northwest quadrant (colored lines) and reconstructed PDSI from grid point 117 (black line) for SDPs identified for that quadrant.

There are some slight variations in the timing of the edge peak relative to when the decrease in the PDSI begins, but the overall pattern indicates that the edge detection filter is successful in identifying changes of state within the index data because for every SDP that appears in any particular quadrant, the edge peak corresponds to a decrease in the

PDSI. PDSI is a measure of drought that utilizes a smoothing filter over a period of 3 to 36 months. The PDSI was developed to include the entire duration of a drought (or wet spell), so that a single abnormally-wet month in the middle of a long-term drought would not have an impact on the PDSI, or even 2 or 3 months with near-normal precipitation following a drought would not necessarily indicate that the drought is over (Dai and NCAR, 2014). This differs from a tree's response to moisture deficits, because a single relatively wet year (relatively wider ring-width) in the middle of a drought period (several relatively thin ring-widths) will be apparent. There are criteria for determining when a drought (or wet spell) is beginning or ending, and the PDSI is adjusted based on these criteria (Alley, 1984; Palmer, 1965). Because the reconstructed PDSI is dependent on a majority of the same tree-ring index data that the edge detection is being applied to, there is an expected correlation between the two (reconstructed PDSI and the edge detection). However, the difference is that PDSI is a cumulative measure of drought whereas the edge detection filter is being used to identify changes in state (wet to dry). The importance of a repeating occurrence of an edge peak at the same time as a decrease in the reconstructed PDSI is that it shows the edge detection filter is finding the onset of the dry periods, and the mapping of this response allows for the identification of the regions where the change is taking place.

To further assess the ability of the edge detection filter to identify the onset of drought, a comparison between drought periods identified in this study (SDPs) versus droughts identified in other tree-ring reconstructed drought analyses was completed. Both the 1930's and 1950's drought periods have been well documented in other studies (Cook et al., 2007; Meko and Woodhouse, 2005; Stahle et al., 2000). The SDPs of 1620AD-

1624AD, 1650AD-1654AD, 1680AD-1686AD, 1726AD-1730AD, 1838AD-1848AD, and 1866AD-1872AD correspond to years identified by Meko and Woodhouse (2005) as drought years for the Blue River Basin (defined by below normal streamflow), which is located in the northern CRB. Stahle et al. (2000) identified the onset of the 16th century megadrought during the 1550's in the southern portion of the CRB, which corresponds to the 1554AD-1562AD SDP identified in this study.

Pattern Recognition

The positive PC loadings (bright green) and negative PC loadings (black) are a measure of the correlation between the site data (either index or edge) with the PC. For any particular PC, sites that have positive loadings are the sites that vary together, while sites that have negative loadings vary together but in the opposite manner. The interpretation of boundaries between positive and negative loadings is they correspond to the divide between different overlying circulation features, which result in different in climatic conditions. This interpretation is based on studies that have shown tree ring-width is dependent on the most limiting factor, such as temperature, precipitation, disease, biological processes, etc. (Cook et al., 2007; Fritts, 1976; Grissino-Mayer, 2014; Meko and Woodhouse, 2005). When trees over such a large geographical area vary in the same manner, the most likely limiting factor is climatic conditions.

The results of the PCA on the index and edge detection output for the SDPs suggest that there are similar circulation patterns forcing the drought intervals. In the case of the Index PCA, PC1 (Fig. 13, left) exhibits a north-south divide between the sites that vary together, and accounts for 47% of the variance. The sites in the central/southern portions of the CRB have negative loadings, while sites in the northern portion of the CRB have positive loadings. This north-south divide pattern is also illustrated in PC2 (Fig. 13, middle), but the signs of the loadings switch from negative to positive in the central/southern portion and from positive to negative in the northern portion of the CRB. Together, these similar patterns account for 84% of the variance in the index data. Based on the interpretation that the PC spatial loading patterns correspond to circulation features, this pattern suggests that a possible atmospheric dipole setup (low pressure center in the north with high pressure center in the central/south, or high pressure center in the north with low pressure center in the central/south) is a common feature that affects variance of tree-ring index values during drought in the CRB.

The results of the edge detection PCA show that PC1 (Fig. 14, left) is characterized by a similar north-south divide pattern as in PC1 and PC2 of the index PCA, and accounts for 60% of the edge variance. The PC1 loading pattern shows that sites within the central/southern portion of the CRB change state (wet to dry) together while sites in the northern portion of the CRB change state (dry to wet) together. This suggests that the possible atmospheric pressure dipole feature is forcing the changes in state. PC2 (Fig. 14, middle) accounts for 27% of the variance, and shows that sites in New Mexico and eastern Colorado change state (dry to wet) together while the remainder of the sites in central, western, and northern portions of the CRB change state (wet to dry) together. This loading pattern suggests there is another type of circulation feature that is forcing changes in state during the SDPs. Based on PC3's loading patter (Fig. 14, right) there may be a third, more complex circulation patter involved in western US drought.

An additional edge PCA was completed only for sites with a continuous record from 1500AD to 1960AD (154 sites), to have the longest temporal coverage. The results are shown in Figure 21(a,b).

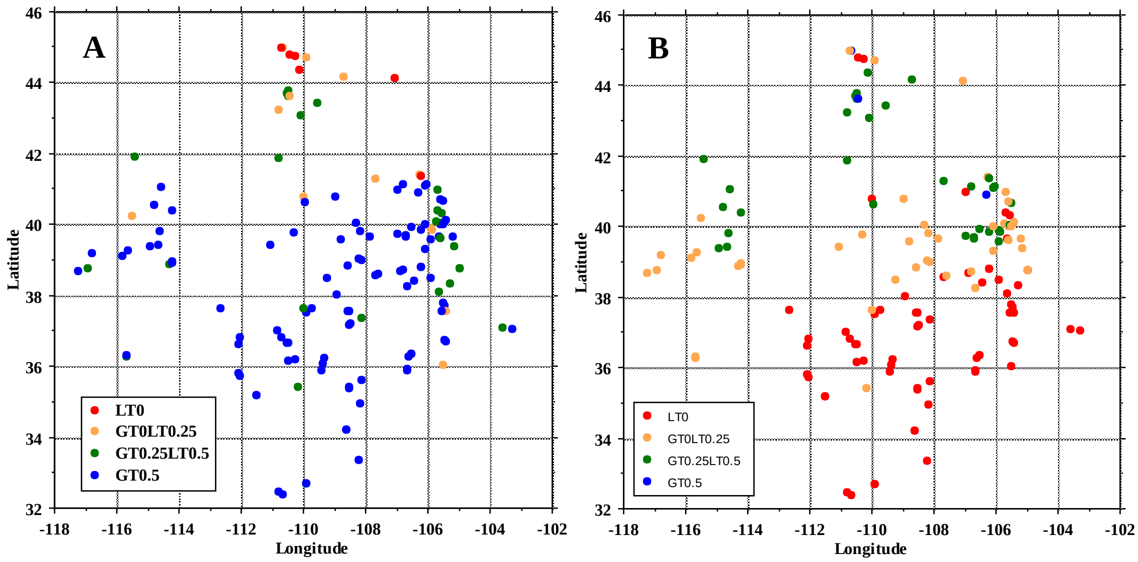

Figure 21. (a) Edge PCA PC1 pattern, (b) edge PCA PC2 pattern. Sites marked with red dots are experiencing loadings less than zero (negative), tan dots represent sites experiencing loadings from 0 to 0.25, green dots represent sites experiencing loadings from 0.25 to 0.5, and blue dots represent sites experiencing loadings greater than 0.5.

The PC1 pattern based on the 154 continuous sites (Fig. 16a) exhibits the same north-south divide as PC1 in Figure 14, with positive loadings in the central/southern CRB and negative loadings to the north. PC2 (Fig. 16b) shows the same northwest-southeast divide as PC2 in Figure 14, with positive loadings to the northwest and negative loadings to the southeast. Since the same patterns emerge using this limited 154 site subset, it can be said that the patterns are both real and robust and recur without significant change over time.

It is well known that anomalous states of SSTs affect the distribution of high- and low-pressure centers around the globe, leading to changes in state with regard to hydroclimatic variables (Cole and Cook, 1998; Cook et al., 2007; Enfield et al., 2001;

Gray et al., 2003; Hoerling and Kumar, 2003; McCabe-Glynn et al., 2013; Tootle et al., 2005). If the patterns of drought onset shown by the edge PCA (Fig. 14) are indeed forced by the overlying circulation features, and the circulation features associated with the patterns in PC's 1 and 2 (Fig. 14, left and middle, which together account for 87% of the variance) are dependent on SSTs, then this suggests that the individual SDPs are forced by similar states of oceanic oscillations.

Mantua et al. (1997) calculated correlation coefficients between December – February precipitation in North America and the PDO index from 1900-1992 (Fig. 22). The results show that the PDO index is positively correlated with precipitation in the southwestern U.S. and northern Mexico, and negatively correlated with precipitation in the northwest U.S. and western Canada. The red box in Figure 22 shows the location of the CRB relative to the correlation analysis. The correlation coefficients exhibit a north-south divide within the red box. The similarities between the PDO - precipitation correlation pattern and the PC1 edge pattern (Fig. 14, left and Fig. 21a) suggest that PC1 is capturing the variance in drought onset as it relates to the PDO.

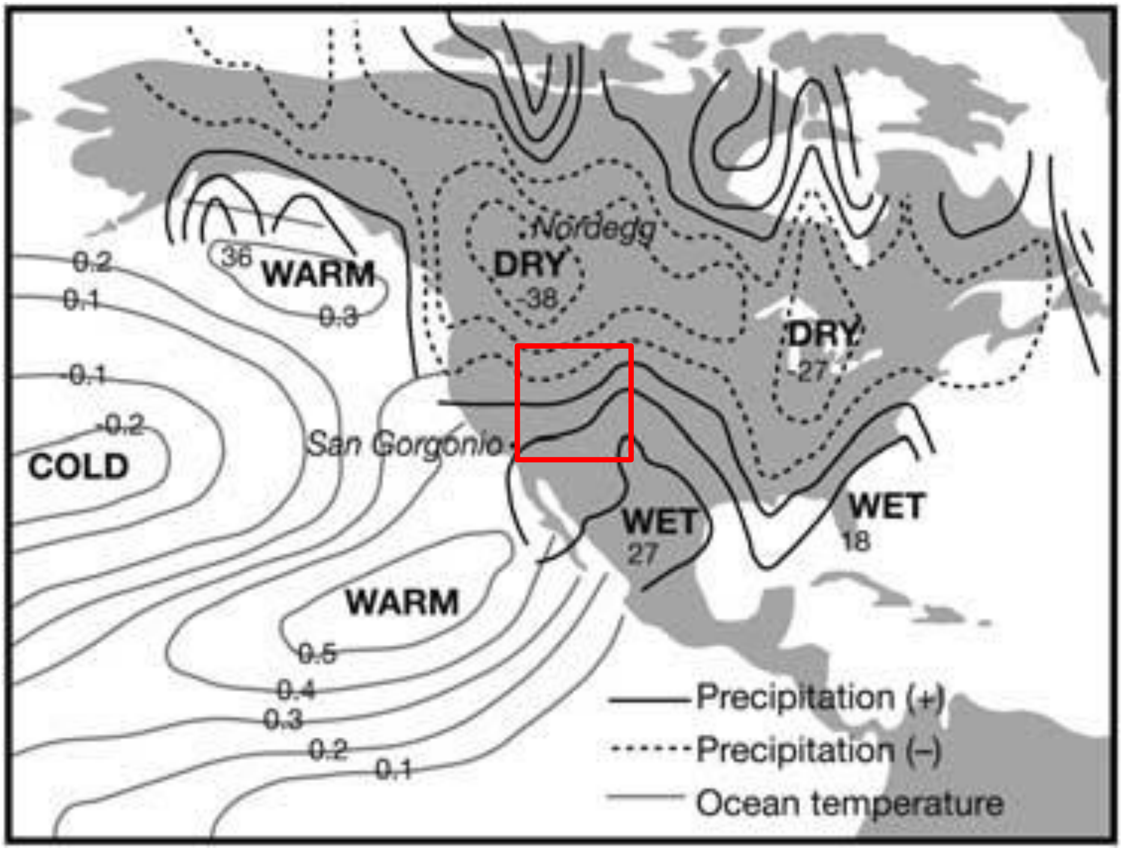

Figure 22. PDO index loading vectors (1945–1993) for Pacific SST's and correlations between North American winter precipitation and the PDO index are shown (from Mantua et al., 1997; Nigam et al., 1999). Red box denotes relative location of the CRB. Location of the San Gorgonio, California and Nordegg, Alberta tree-ring sampling sites used by MacDonald and Case (2005) are shown also.

Enfield et al. (2001) calculated correlation coefficients between the AMO index and climate division rainfall in the U.S. (Fig. 23). In Figure 23, climate division precipitation within the CRB is negatively correlated with AMO, where the highlighted dots indicate correlation above the 90% significance level. In the Enfield et al. (2001) analysis, the southwest and northeast portions of the CRB experience strong negative correlations between precipitation and AMO. These areas correspond to the areas in PC2 (Fig. 14, middle) that experience large, positive loadings (Arizona and Northern Colorado). However, a strong negative correlation is not present in the northwest portion of the CRB (Fig. 23), while at the same time there are large and positive loadings in the northwest CRB in PC2 of Figure 14 (middle). This discrepancy may be influenced by the relative size of the climatic divisions in this area with precipitation values assigned to an entire climate division possibly not representing the conditions at a particular site because climate division boundaries do not necessarily have to correspond to actual transitions between climate types. So, these similarities indicate that the pattern in PC2 (Fig. 14) is likely capturing the variance in the edge data due to circulation patterns forced by the AMO.

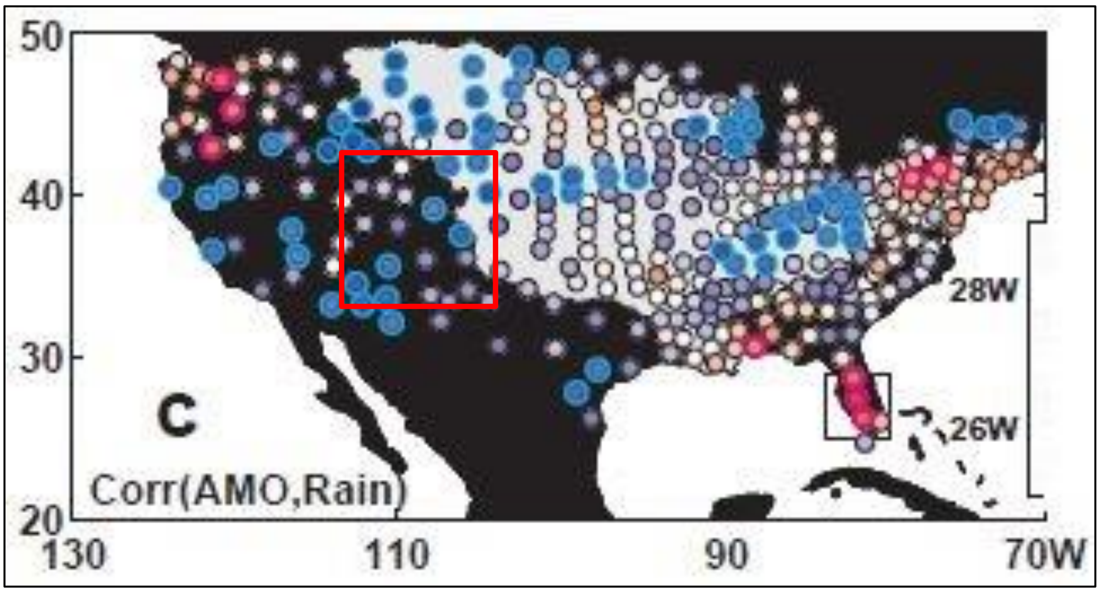

Figure 23. Correlation of the AMO index with climate division rainfall (from Enfield et al., 2001). Positive correlations are marked with red dots, and negative correlations are marked with blue dots. The larger highlighted circles indicated correlations above the 90% confidence level. The red box shows the location of the CRB.

Figure 24(a-l) shows the reconstructed state of oceanic oscillations for each SDP starting with 1630AD-1638AD (due to length constraints on some of the reconstruction data).

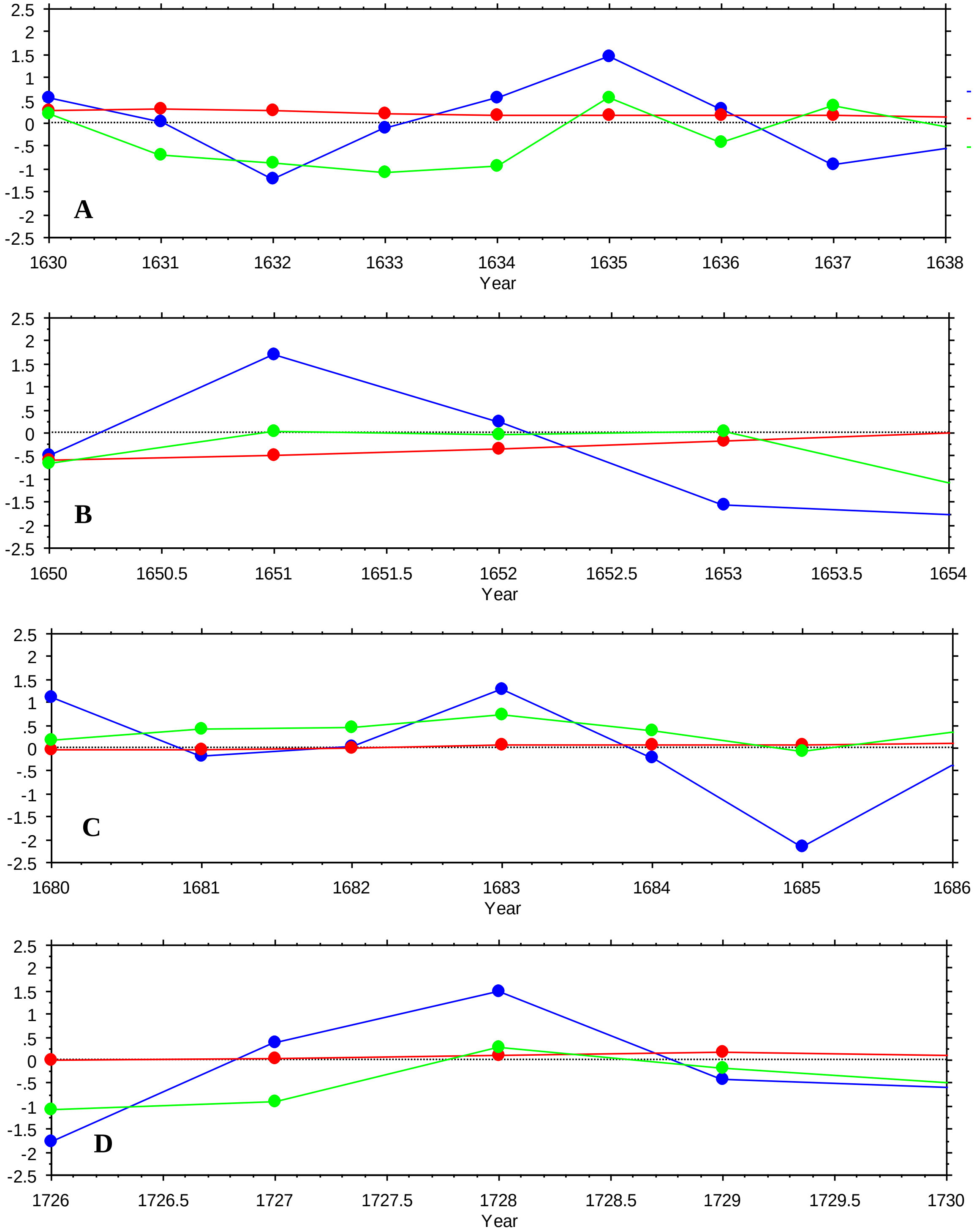
A
2.5 2 1.5 1 .5 0 -.5 -1 -1.5 -2 -2.5
1630 1631 1632 1633 1634 1635 1636 1637 1638
Year
B
2.5 2 1.5 1 .5 0 -.5 -1 -1.5 -2 -2.5
1650 1650.5 1651 1651.5 1652 1652.5 1653 1653.5 1654
Year
C
2.5 2 1.5 1 .5 0 -.5 -1 -1.5 -2 -2.5
1680 1681 1682 1683 1684 1685 1686
Year
D
2.5 2 1.5 1 .5 0 -.5 -1 -1.5 -2 -2.5
1726 1726.5 1727 1727.5 1728 1728.5 1729 1729.5 1730
Year

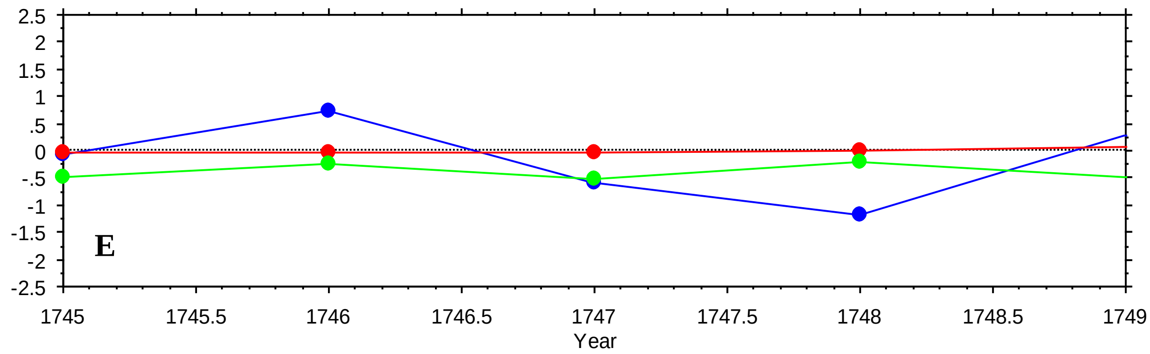
E
2.5
2
1.5
1
.5
0
-.5
-1
-1.5
-2
-2.5
1745
1745.5
1746
1746.5
1747
1747.5
1748
1748.5
1749
Year

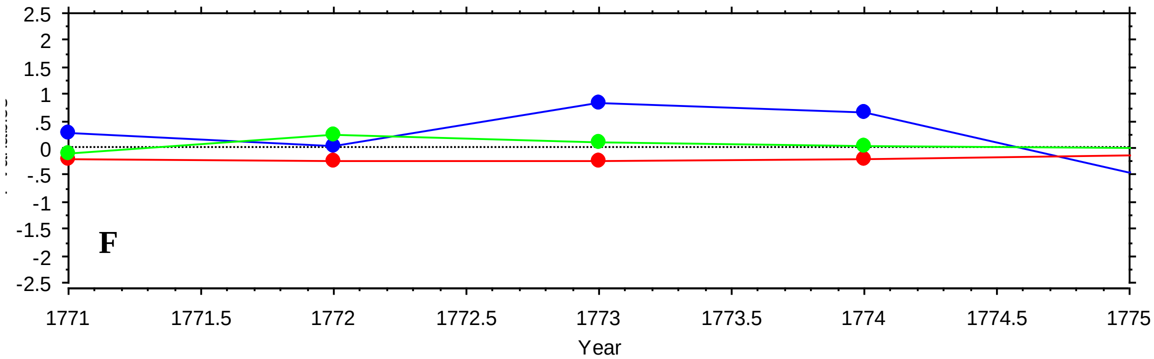
F
2.5
2
1.5
1
.5
0
-.5
-1
-1.5
-2
-2.5
1771
1771.5
1772
1772.5
1773
1773.5
1774
1774.5
1775
Year

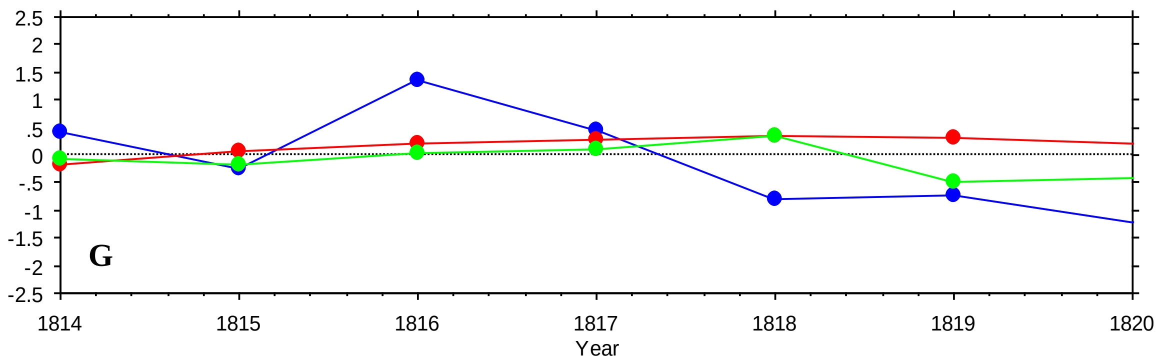
G
2.5
2
1.5
1
.5
0
-.5
-1
-1.5
-2
-2.5
1814
1815
1816
1817
1818
1819
1820
Year

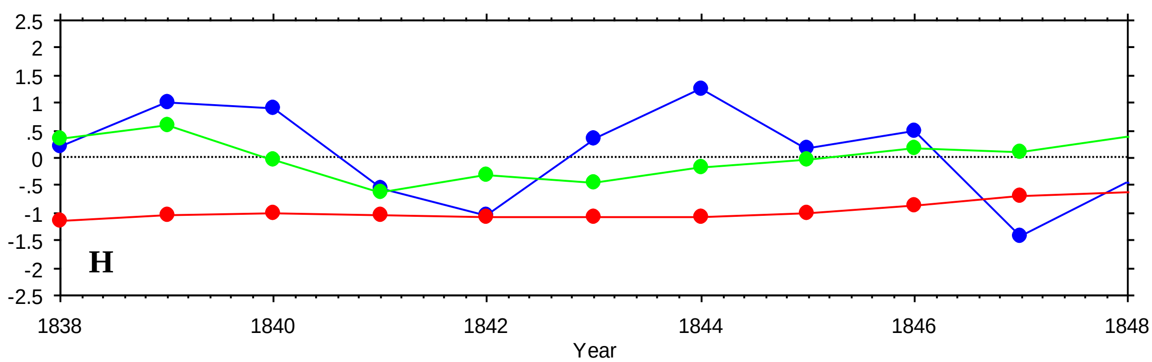
H
2.5
2
1.5
1
.5
0
-.5
-1
-1.5
-2
-2.5
1838
1840
1842
1844
1846
1848
Year

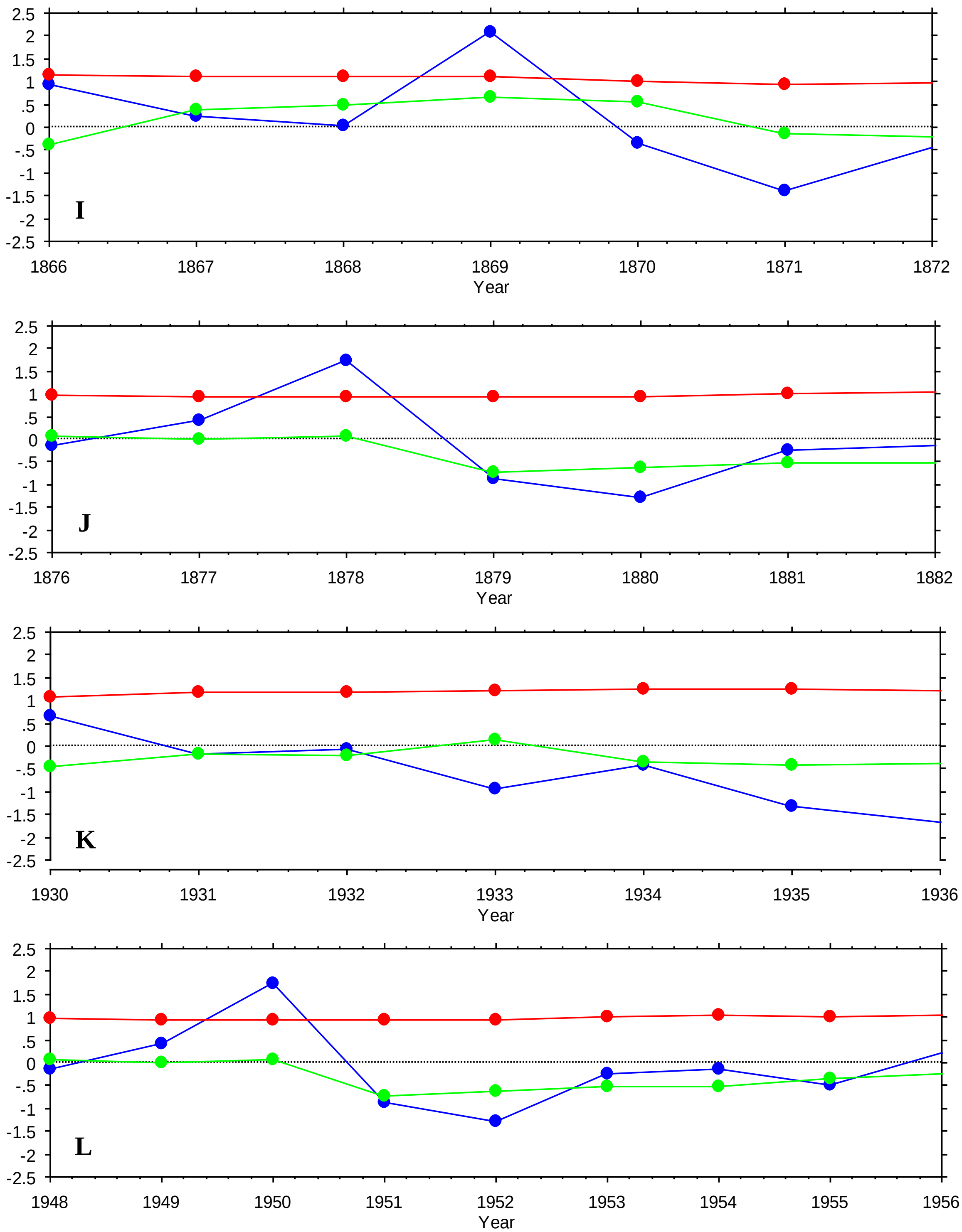

Figure 24(a-l). Reconstructed oceanic oscillation indices for each SDP (a through l, respectively) beginning with the year 1630AD. Nino3.4 index (SST anomalies) (blue), AMO index (red), and PDO index (green). Y-axis is the standardized index value.

Tree-ring chronologies used in the reconstruction of the AMO index were located in the southeastern United States, Northern Scandinavia, the Mediterranean, and Eastern Egypt/Jordan (Gray et al., 2004). The data used to reconstruct the PDO index was derived from tree-ring chronologies located in southern California, western Canada, southern Alaska, and eastern China (Biondi et al., 2001; D'Arrigo et al., 2001; MacDonald and Case, 2005; Shen et al., 2006). The data used to reconstruct Nino3.4 Index (SST anomalies) was from tree-ring chronologies located in the tropics and mid-latitude of both hemispheres (Li et al., 2013), corals from the central Pacific, tree-ring chronologies from the Texas-Mexico border region, corals plus tree-rings from the tropics (Wilson et al., 2010), and tree-ring chronologies spanning the coterminous United States from the North American Drought Atlas (Li et al., 2011). The state of oceanic oscillations was compared to the peak index and edge years listed in Table B2 in Appendix B. The most common combination of oscillation indices that occurred during the peak edge and peak index years was negative Nino3.4 index (SST anomalies), negative PDO index, and positive AMO index, occurring 8 out of 12 instances. Instrumental data and the results from the analysis of drought frequency by McCabe et al. (2004) supports that this combination of indices corresponds to drought in the CRB (Gray et al., 2004; NOAA ESRL, 2015).

Drought Classification

Comparing the edge migration of the 1726AD-1730AD SDP (Fig. 11) to the edge migration of the 1948AD-1956AD SDP (Fig. 12), it is apparent that there are significant differences between the two. While no two SDPs have an identical edge migration pattern, similarities between the SDPs, and thus the potential for categorization, lie in the common areas affected by drought onset. These are the patterns represented in the edge PCA's (Fig. 14 and Fig. 21). Based on the variance accounted for by PC1, the central and southern portions of the CRB are the areas that experience drought onset the most. PC2 in Figure 14 shows that the second most common drought onset pattern includes the central and western portions of the CRB. The patterns illustrated in PC1 (Fig. 14, left) and PC2 (Fig. 14, middle) are the most significant drought onset patterns, accounting for 87% of the variance in the edge data. Mapping PC1 (PDO-type) and PC2 (AMO-type) loadings temporally allows for the discrimination of the PDO and AMO influence on each SDP.

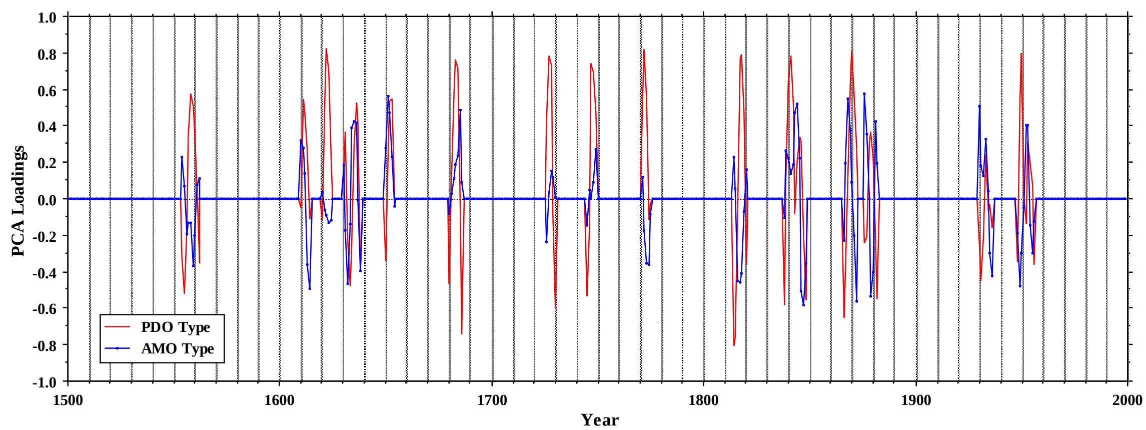

Figure 25. PDO-type (PC1) loadings (red line) and AMO-type (PC2) loadings (blue) for each SDP from 1500AD – 1960AD. This analysis only includes the 154 sites with continuous records.

The PDO-type loadings exhibit a consistent maximum for each SDP, which indicates that PDO has a similar influence on the drought onset pattern for almost every SDP. Also, the mean spacing between each of the SDPs is about 20-30 years, which corresponds to the accepted episodic oscillation of 25 years for PDO. In contrast, AMO-type loadings have periods of strong positive loadings (mid- to late-1600's and mid- to late-1800's) and periods of relatively weak positive loadings (mid-1700's). This amplitude-modulated pattern is also present in AMO index reconstructions. Figure 26 shows the reconstructed AMO index from Gray et al. (2004) for the period of study.

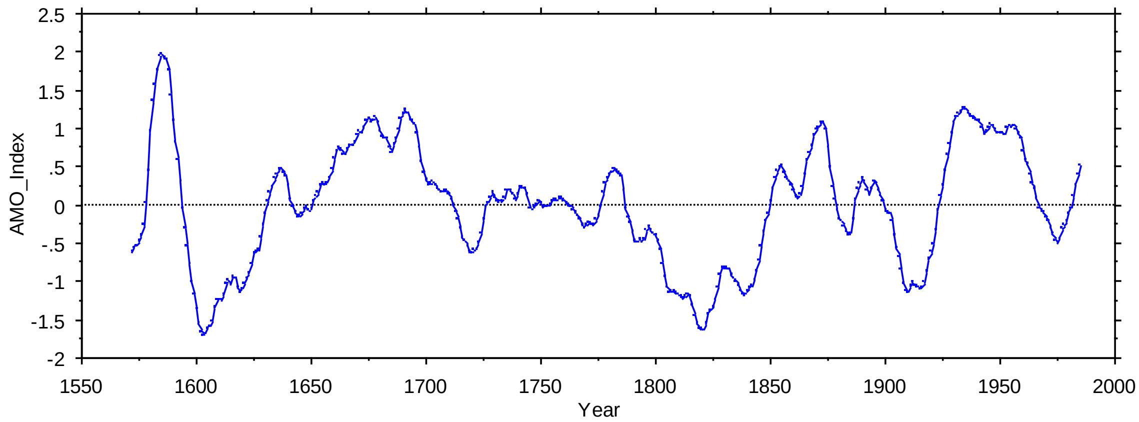

Figure 26. Reconstructed AMO index from Gray et al. (2004).

There is a strong, positive AMO index during the late 1600's and late 1800's, which corresponds to the periods in Figure 25 when AMO has a stronger influence on drought onset, as indicated by the strong, positive AMO-type loadings. During the mid-1700's, the reconstructed AMO index is relatively neutral. This corresponds to the timing of relatively weak, positive AMO-type loadings seen in Figure 25 with PDO providing the majority of the forcing on the drought onset pattern. Therefore, the AMO index strength plays a critical role in how much influence Atlantic oceanic oscillations, as quantified in the AMO index, have on drought onset patterns in the CRB.

Superposed Epoch Analysis shows that the edge detection for each SDP has the same general pattern, with only slight differences between each SDP. As illustrated in Figure 16, some of the SDPs have one sharp edge peak, which indicates there is one year of a significant change in state, where others have a smoothed edge peak with multiple large, positive edge values in a row, indicating an initial change of state followed by a continued change of state of similar magnitude acting to intensify the drought.

Chapter 6

Conclusions and Future Research

Using an edge detection filter, occurrences of drought onset in the CRB were identified and characterized in terms of their spatial patterns and migration vectors. The SDP edge PC1 patterns (Fig. 14, left and Fig. 21a) support the idea of an atmospheric pressure dipole (forced by changes in oceanic oscillations) acting as the main control on the variance of changes in state from wet to dry conditions within each SDP in the CRB. This pattern is very similar to the north-south dipole present in the CRB during the negative phase of PDO. PC 2 (Fig. 14, middle, and Fig. 21b) suggest that there is a second atmospheric circulation pattern in addition to this dipole that plays a role in drought onset as well, likely a circulation pattern forced by the positive phase of AMO. Mapping of the PC1 and PC2 loadings temporally further suggests that PDO and AMO are the leading forcing mechanisms for drought onset patterns in the CRB. Therefore, even though the majority of the SDPs have the same oceanic oscillation index setup that is ultimately forcing drought onset, these droughts are different. There are differences in the timing of the peak index year relative to the onset of drought (Table B2, Appendix B), there are differences in magnitude (as evidenced by the species analysis in Fig. 19), and there are differences in the edge migration patterns.

The edge detection filter could also be applied to different types of tree-ring analysis, such as earlywood-width, latewood-width, or wood density. This may allow for a seasonal distinction between drought onset patterns. It would also be beneficial to apply this technique to the tree-ring records in the CRB dating back to the early 12th century to analyze the onset pattern of the single greatest megadrought to determine if the edge was similar or different from those within the past 500 years (Cook et al., 2007).

Within the CRB, there is a responsibility to balance economic interests, environmental management, and water law (Pulwarty and Melis, 2001). This balance is affected by changes in water availability, and controls on its variability, which include climate (Pulwarty and Melis, 2001). The results presented in this paper are a useful starting point for improving drought predictability, and possibly aiding in water management decisions during times of drought onset. For instance, the patterns shown in the PCA analysis provide insight as to which areas in the CRB are affected by drought the most, and how these sites vary together. If a pattern similar to that of PC1 in Figure 14 (left) begins to emerge with respect to a decrease in precipitation at meteorological observation stations, and the state of oceanic oscillation indices is known, it is possible to know the general region within the CRB that will most likely experience similar conditions.

A more detailed analysis between the edge patterns and individual drought periods and their duration could result in improved drought predictability. For example, if a particular drought onset pattern develops, could this be indicative of how long the drought will last? 3 years? 5 years? 10 years? Applying the GISS GCM 2100 scenario with economic development, Lane et al. (1999) found that the major overall impacts of global warming in the United States occur in the west, and include more stress on available water due to increases in total withdrawals and, in some areas, decreases in stream flows. An enhanced ability to better predict drought patterning and duration in the currently over appropriated Colorado River Basin becomes increasingly more important when considering the effect of global warming on future availability and wise use of scarce water resources.

Appendix A

Equations

Equation 1. The Gaussian smoothing equation applied to a tree-ring index value in a particular year, where NM587 represents the index value for that particular year. The resulting smoothed index value for that year takes into account the index values of the 2 years prior and the 2 years post the year of interest.

```
NM587gaussian =
SUM(LAG(NM587,-2),(LAG(NM587,-1)*2),(NM587*5),(LAG(NM587,1)*2),LAG(NM587,2))
```

Equation 2. The edge detection equation applied to the output of the Gaussian smoothing equation (Equation 1), where NM587gaussian is the smoothed index value for a particular ‘year of interest’. The edge detection takes into account the change in smoothed index magnitude from the year before the ‘year of interest’ to the year after the ‘year of interest’. The edge weightings were assigned based on the Canny (1986) description of a step-impulse response edge detector.

```
NMedge =
SUM((LAG(NM587gaussian,-1)*-2),(NM587gaussian*0),(LAG(NM587gaussian,1)*2))
```

Appendix B

Tables

Table B1. PDSI grid point and number of tree-ring site files within each quadrant.

Quadrant	PDSI Grid Point	Number of Site Files
New Mexico – Southwest	120	29
New Mexico – Northwest	119	53
New Mexico – Northeast	133	21
Colorado – Southwest	118	37
Colorado – Northwest	117	22
Colorado – Northeast	131	67
Colorado – Southeast	132	20
Arizona – Northwest	88	41
Arizona – Northeast	104	30
Arizona – Southeast	105	53
Nevada – Southeast	73	3
Nevada – Eastern	72	17
Nevada – Northeastern	71	6
Utah – Southwest	87	2
Utah – Northeast	102	9
Utah – Southeast	103	6
Wyoming – Western	101	23
Wyoming – Central/Eastern	116/130	13

Table B2. Peak edge years and peak index years within each specified drought period. A peak year was calculated by averaging only the site files within the quadrants that experienced drought onset during that particular specified drought period. The peak edge year is defined as the year within the specified drought period with the maximum average edge value, and the peak index year is defined as the year within the specified drought period with the lowest average index value.

Specified Drought Period	**Peak Edge Year**	**Peak Index Drought Year**
1554AD-1562AD	1557	1561
1610AD-1614AD	1612	1613
1620AD-1624AD	1622	1624
1630AD-1638AD	1630	1632
1650AD-1654AD	1653	1654
1680AD-1686AD	1684	1685
1726AD-1730AD	1728	1729
1745AD-1749AD	1747	1748
1771AD-1775AD	1772	1773
1814AD-1820AD	1817	1819
1838AD-1848AD	1840	1842
1866AD-1872AD	1870	1871
1876AD-1882AD	1879	1880
1930AD-1936AD	1933	1934
1948AD-1956AD	1950	1954

Table B3. Number of tree-ring site files included in each 100-year period. Site files that did not have a complete record for the entire 100-year period were not used for that particular period.

100-Year Period	Number of Site Files used in Spatial Analysis
Index 1900-1999	434
Index 1800-1899	422
Index 1700-1799	385
Index 1600-1699	255
Index 1500-1599	154
Edge 1900-1999	432
Edge 1800-1899	423
Edge 1700-1799	385
Edge 1600-1699	254
Edge 1500-1599	154

Table B4. Tree species codes (WSL, 2012), the dominant sensitivity of the species (Scuderi, 2015), and the number of site files per species used in statistical analysis.

Species Code	**Species Name**	**Precip. vs. Temp. Sensitive**	**Number of Site Files**
PIED	Colorado Pinyon, Colorado Pinyon pine, Pinyon, and Pinyon pine	Precipitation sensitive	88
PIMO	Single Leaf Pinyon	Precipitation sensitive	13
PIPO	Ponderosa pine	Precipitation sensitive	130
PSME	Douglas fir	Precipitation sensitive	119
PCEN	Engelmann spruce, Mountain spruce, Silver spruce, and White spruce	Precipitation and Temperature sensitive	27
PIFL	Limber pine	Temperature sensitive	16
PILO	Great Basin Bristlecone pine, Intermountain Bristlecone pine, and Western Bristlecone pine	Temperature sensitive	11

References

Adams, D.K., and A.C. Comrie, 1997: The North American Monsoon. *Bulletin of the American Meteorological Society*, **78**, 2197-2213.

Ali, M., and D. Clausi, 2001: Using the Canny Edge Detector for Feature Extraction and Enhancement of Remote Sensing Images. *IEEE*, 2298-2300.

Alley, W. M., 1984: The Palmer Drought Severity Index: Limitations and Assumptions. *Journal of Climate and Applied Meteorology*, **23**, 1100 – 1109.

Alley, W. M., 1985: The Palmer Drought Severity Index as a measure of hydrologic drought. *Water Resources Bulletin: American Water Resources Association*, **21**.

ArcGIS_1, 2012: ArcGIS Resources: How inverse distance weighted interpolation works. [Available online at http://resources.arcgis.com/en/help/main/10.1/index.html#//00310000002m000000.] Accessed March 15, 2015.

ArcGIS_2, 2012: ArcGIS Resources: How Principal Components works. [Available online at http://resources.arcgis.com/en/help/main/10.1/index.html#/How_Principal_Components_works/009z000000qm000000/.] Accessed March 15, 2015.

ArcGIS, 2013: ArcGIS Resources: Kriging in Geostatistical Analyst. [Available online at http://help.arcgis.com/en/arcgisdesktop/10.0/help/index.html#//003100000032000000.] Accessed March 15, 2015.

Biondi, F., A. Gershunov, and D.R. Cayan, 2001: North Pacific Decadal Climate Variability since 1661. *Journal of Climate*, **14**, 5-10.

Canny, J., 1986: A computational approach to edge detection. *Transactions on Pattern Analysis and Machine Intelligence*, **PAMI-8**, 679-697.

Cayan, D., T. Das, D. Pierce, T. Barnett, M. Tyree, and A. Gershunov, 2010: Future dryness in the southwest US and the hydrology of the early 21st century drought. *Proceedings of the National Academy of Sciences of the United States of America*, **107**, 21271-21276.

Cole, J., and E. Cook, 1998: The changing relationship between ENSO variability and moisture balance in the continental United States. *Geophysical Research Letters*, **25**, 4529-4532.

Cook, E.R., D.M Meko, D.W. Stahle, and M.K. Cleaveland, 1999: Drought Reconstructions for the Continental United States. *Journal of Climate*, **12**, 1145-1162.

Cook, E.R. and P.J. Krusic, 2004: The North American Drought Atlas. Lamont-Doherty Earth Observatory and the National Science Foundation. [Available at http://iridl.ldeo.columbia.edu/SOURCES/.LDEO/.TRL/.NADA2004/.pdsi-atlas.html.]

Cook, E.R., R. Seager, M.A. Cane, and D.W. Stahle, 2007: North American drought: Reconstructions, causes, and consequences. *Earth-Science Reviews*, **81**, 93-134.

CPC (Climate Prediction Center), 2012: Climate Prediction Center, Warm (El Nino/Southern Oscillation – ENSO) Episodes in the Tropical Pacific. [Available online at http://www.cpc.ncep.noaa.gov/products/analysis_monitoring/impacts/warm_impacts.shtml.] Accessed March 18, 2014.

D'Arrigo, R., R. Villalba, and G. Wiles, 2001: Tree-ring estimates of Pacific decadal climate variability. *Climate Dynamics*, **18**, 219-224.

Dai, A., and National Center for Atmospheric Research (NCAR) Staff (Eds). Last modified 21 Mar 2014. "The Climate Data Guide: Palmer Drought Severity Index (PDSI)." [Available online at https://climatedataguide.ucar.edu/climate-data/palmer-drought-severity-index-pdsi.]

Dean, J.S., W.J. Robinson, D.O. Bowden, and M.K. Cleaveland, 2015: Bobcat Canyon. [https://www.ncdc.noaa.gov/paleo/study/3063.] Accessed March 25, 2015.

Enfield, D.B., A.M. Mestas-Nunez, and P.J. Trimble, 2001: The Atlantic multidecadal oscillation and its relation to rainfall and river flows in the continental U.S. *Geophysical Research Letters*, **28**, 2077-2080.

FAO (Food and Agriculture Organization), 1983. Guidelines: Land evaluation for Rain fed Agriculture. FAO Soils Bulletin 52, Rome.

Fritts, H. C., 1976: *Tree Rings and Climate*. Academic Press, 567pp.

Fye, F.K., D.W. Stahle, and E.R. Cook, 2003: Paleoclimate Analogs to Twentieth-Century Moisture Regimes across the United States. *Bulletin of the American Meteorological Society*, 901-909.

Gray, S.S.L., 2003: Persistent Drought in the Colorado River Basin. [Available online at http://scholar.google.com/scholar?hl=en&q=persistent+drought+in+the+colorado+river+basin&btnG=&as_sdt=1%2C32&as_sdtp=]

Gray, S.T., J.L. Betancourt, C.L. Fastie, and S.T. Jackson, 2003: Patterns and sources of multidecadal oscillations in drought-sensitive tree-ring records from the central and southern Rocky Mountains. *Geophysical Research Letters*. **30**. doi: 10.1029/2002GL016154.

Gray, S.T., L.J. Graumlich, J.L. Betancourt, and G.T. Pederson, 2004: A tree-ring based reconstruction of the Atlantic Multidecadal Oscillation since 1567 A.D. *Geophysical Research Letters*, **31**, L12205, doi:10.1029/2004GL019932.

Grissino-Mayer, H. D. (1996). A 2129-year reconstruction of precipitation for northwestern New Mexico, USA. *In* “Tree Rings, Environment, and Humanity” (J. S. Dean, D. M. Meko, and T. W. Swetnam, Eds.), *Radiocarbon* 1996, Department of Geosciences, Univ. of Arizona, Tucson: pp. 191–204.

Grissino-Mayer, H.D., 2014: Principles of Dendrochronology. [Available online at http://web.utk.edu/~grissino/principles.htm#def.] Accessed March 25, 2015.

Haurwitz, M.W., and G.W. Brier, 1981: A Critique of the Superposed Epoch Analysis Method: Its Application to Solar–Weather Relations. *Monthly Weather Review*, **109**, 2074–2079. doi: http://dx.doi.org/10.1175/1520-0493(1981)109<2074:ACOTSE>2.0.CO;2

Heim, R., 2002: A review of twentieth-century drought indices used in the United States. *Bulletin of the American Meteorological Society*. 1149-1165.

Held, I.M., and B.J. Soden, 2006: Robust responses of the hydrological cycle to global warming. *Journal of Climate*, **19(21)**, 5686-5699.

Hidalgo, H.G., 2004: Climate precursors of multidecadal drought variability in the western United States. *Water Resources Research*, **40**, doi:10.1029/2004WR003350.

Hoerling, M., and A. Kumar, 2003: The Perfect Ocean for Drought. *Science*, **299**, 691-694.

IPCC [Stocker, T.F., D. Qin, G.-K. Plattner, M. Tignor, S.K. Allen, J. Boschung, A. Nauels, Y. Xia, V. Bex, and P.M. Midgley], 2013: *Climate Change 2013: The Physical Science Basis. Contribution of Working Group 1 to the Fifth Assessment Report of the Intergovernmental Panel on Climate Change.* Cambridge University Press, 1535 pp.

ITRDB, 2014: Contributors of the International Tree-Ring Data Bank, IGBP PAGES/World Data Center For Paleoclimatology, NOAA/NCDC Paleoclimatology Program, Boulder, Colorado, USA.

ITRDB, 2015: Tree Ring Data Description: Description of Tree Ring Data and Procedures. [Available online at ftp://ftp.ncdc.noaa.gov/pub/data/paleo/treering/treeinfo.txt.] Accessed March 25, 2015.

Kim, T., C. Yoo, and J. Ahn, 2008: Influence of climate variation on seasonal precipitation in the Colorado River Basin. *Stoch. Environ. Res. Risk Assess.*, **22**, 411-420.

Lane ME, Kirshen PH, Vogel RM (1999) Indicators of impacts of global climate change on U.S. water resources. *Journal of Water Resources Planning and Management*, 125, 194–204.

Li, J., S. Xie, E.R. Cook, G. Huang, R. D'Arrigo, F. Liu, J. Ma, and X. Zheng, 2011: Interdecadal modulation of El Nino amplitude during the past millennium. *Nature Climate Change*, **1**, 114-118.

Li, J. S. Xie, E.R. Cook, M.S. Morales, D.A. Christie, N.C. Johnson, F. Chen, R. D'Arrigo, A.M. Fowler, X. Gou, and K. Fang, 2013: El Nino modulations over the past seven centuries. *Nature Climate Change*, **3**, doi:10.1038/nclimate1936.

Lim, J. S., 1990: Two Dimensional Signal and Image Processing. *Prentice Hall*, Englewood Cliffs, New Jersey.

MacDonald, G.M., and R.A. Case, 2005: Variations in the Pacific Decadal Oscillation over the past millennium. *Geophysical Research Letters*, **32**, doi:10.1029/2005GL022478.

Mantua, N.J., S.R. Hare, Y. Zhang, J.M. Wallace, and R.C. Francis, 1997: A Pacific Interdecadal Climate Oscillation with Impacts on Salmon Production. *Bulletin of the American Meteorological Society*, **78**, 1069-1079.

McCabe, G.J., M.A. Palecki, and J.L. Betancourt, 2004: Pacific and Atlantic Ocean influences on multidecadal drought frequency in the United States. *PNAS*, **101**, 4136 – 4141.

McCabe-Glynn, S., K.R. Johnson, C. Strong, M. Berkelhammer, A. Sinha, H. Cheng, and R.L. Edwards, 2013: Variable North Pacific influence on drought in southwestern North America since AD 854. *Nature Geoscience*, **6**. doi: 10.1038/ngeo1862.

Meko, D.M., and C.A. Woodhouse, 2005: Tree-ring footprint of joint hydrologic drought in Sacramento and Upper Colorado River basins, western USA. *Journal of Hydrology*, **308**, 196-213.

Meko, D.M., C.A. Woodhouse, C.A. Baisan, T. Knight, J.J. Lukas, M.K. Hughes, and M.W. Salzer, 2007: Medieval drought in the upper Colorado River Basin. *Geophysical Research Letters*, **34**. doi: 10.1029/2007GL029988.

Miller, W.P., and T.C. Piechota, 2008: Regional Analysis of Trend and Step Changes Observed in Hydroclimatic Variables around the Colorado River Basin. *Journal of Hydrometeorology*, **9**, 1020-1034.
Mishra, A.K., and V.P. Singh, 2010: A review of drought concepts. *Journal of Hydrology*, **391**, 202-216.
NCDC (National Climatic Data Center), 2014: Tree Ring Data Description. [Available online at http://www.ncdc.noaa.gov/paleo/treeinfo.html.] Accessed March 23, 2014.
Nigam, S., M. Barlow, and E.H. Berbery, 1999: Analysis links Pacific decadal variability to drought and streamflow in United States. *Eos Trans. AGU*, **80**, 621, 622, 625.
NOAA ESRL (National Oceanic and Atmospheric Administration, Earth Systems Research Laboratory), 2015: Climate Indices: Monthly Atmospheric and Ocean Time Series. [Available online at http://www.esrl.noaa.gov/psd/data/climateindices/list/]. Accessed April 4, 2015.
North, G.R., T.L. Bell, and R.F. Cahalan, 1982: Sampling Errors in the Estimation of Empirical Orthogonal Functions. *Monthly Weather Review*, **110**, 699-706.
Palmer, W.C., 1965: Meteorological Drought. *U.S. Weather Bureau Research Paper No. 45*, 58.
Pulwarty, R.S., and T.S. Melis, 2001: Climate extremes and adaptive management on the Colorado River: Lessons from the 1997-1998 ENSO event. *Journal of Environmental Management*, **63**, 307-324.
SAS Institute, 1999. *StatView: StatView reference*. SAS Inst.
Scuderi, Louis, 2015. Personal communication on the topic of precipitation- versus temperature- sensitive trees.
Shen, C., W. Wang, W. Gong, and Z. Hao, 2005: A Pacific Decadal Oscillation record since 1470 AD reconstructed from proxy data of summer rainfall over eastern China. *Geophysical Research Letters*, **33**, doi:10.1029/2005GL024804.
Sheppard, P.R., A.C. Comrie, G.D. Packin, K. Angersbach, and M.K. Hughes, 2002: The climate of the U.S. Southwest. *Climate Research*, **21**, 219-238.
Smith, L.I., 2002: *A Tutorial on Principal Components Analysis*. [Available online at http://csnet.otago.ac.nz/cosc453/student_tutorials/principal_components.pdf.] Accessed April 2, 2015.
Stahle, D.W., E.R. Cook, M.K. Cleaveland, M.D. Therrell, D.M. Meko, H.D. Grissino-Mayer, E. Watson, and B.H. Luckman, 2000: Tree-ring Data Document 16th Century Megadrought Over North America. *Eos*, **81**, 121-132.
Tootle, G., T. Piechota, and A. Singh, 2005: Coupled oceanic-atmospheric variability and U.S. streamflow. *Water Resources Research*, **41**, W12408, doi: 10.1029/2005WR004381.
Williams, A.P., C.D. Allen, C.I. Millar, T.W. Swetnam, J. Michaelsen, C.J. Still, and S.W. Leavitt, 2010: Forest responses to increasing aridity and warmth in the southwestern United States. *PNAS*, **107**, 21289-21294.
Wilson, R., E. Cook, R. D'Arrigo, N. Riedwyl, M.N. Evans, A. Tudhope, and R. Allan, 2010: Reconstructing ENSO: the influence of method, proxy data, climate forcing and teleconnections. *Journal of Quaternary Science,* **25**, 62-78.

WMO (World Meteorological Organization), 1986. World Meteorological Organization (WMO), 1986. Report on Drought and Countries Affected by Drought during 1974-1985, WMO, Geneva, p.118.

Woodhouse, C.A., and J.T. Overpeck, 1998: 2000 years of drought variability in the central United States. *Bulletin of the American Meteorological Society*, **79**, 2693-2714.

Woodhouse, C.A., D.M. Meko, G.M. MacDonald, D.W. Stahle, and E.R. Cook, 2009: A 1,200-year perspective of 21st century drought in southwestern North America. *PNAS*, **107**, 21283-21288.

WSL (Swiss Federal Institute for Forest, Snow and Landscape Research), 2012: Dendrochronology species database. [Available online at http://www.wsl.ch/dendro/products/dendro_species/index_EN.] Accessed March 31, 2015.